Chapter 3

Analytical solutions

In general, **flow and heat transport problems can only be solved analytically for special cases**. Such cases are characterized as follows:

- Constant coefficients of the flow and heat transport equation and of the boundary conditions and therefore homogeneous porous media are assumed. In the case of heat transport, this usually means constant thermal retardation or thermal velocity and constant thermal diffusion and dispersion coefficients.
- The flow domain is sufficiently simple, for example, infinite, or radially symmetric.
- The initial condition is sufficiently simple, for example, constant, or zero.
- The boundary conditions are sufficiently simple, for example, constant, or zero.

If these conditions are met to some degree, analytical solutions are, in general, preferable over numerical ones. Important applications of analytical solutions are **analytical approximations** to complex situations, the **determination of parameters** using experimental data, or the **test of numerical solution methods**, like the finite difference, the finite volume, or the finite element methods.

For heat transport, in general, analytical solutions are restricted to closed systems. Nevertheless, analytical approximations are available for both open- and closed-loop systems. There exists a long tradition in using **analytical solutions** for groundwater flow, and mass diffusion, solute transport, and heat transport problems in porous media and in fluids. In the following literature overview, we list a few representatives in the field of heat transport in solid materials, saturated porous media, and groundwater.

Carslaw and Jaeger (1946, 1959) presented a large number of analytical solutions to the problem of heat conduction in solid materials. Many of these solutions are used in the field of both water flow (exploiting the analogy to piezometric head diffusion) and heat transport in groundwater.

Ingersoll et al. (1948, 1954) presented a comprehensive theory and analytical solutions to the heat conduction problem with engineering and geological applications. Among other subjects, they treated the mathematical problem of heat sources for heat pumps.

Domenico and Palciauskas (1973) offer analytical solutions to the steady-state flow and heat transport problem in homogeneous rectangular vertical regions using concepts from Toth (1963). The upper boundary condition is a prescribed head condition that represents the water table. The lateral and lower boundaries are impermeable.

Gringarten and Sauty (1975) investigated the transient temperature evolution of a pumped aquifer during reinjection of water at a temperature different from that of the native water. A horizontal aquifer of constant thickness with impermeable bottom and top layers is considered. Flow is assumed to be at steady state, thus neglecting the short transient period during reinjection. Flow direction is arbitrary. Transient heat transport is solved semianalytically for the curved stream channel between the two wells, using the stream function concept and taking into account heat flow from cap rock and bedrock. Results are given in dimensionless form.

Mercer et al. (1982) reviewed a series of analytical solutions for aquifer thermal energy storage.

Uffink (1983) investigated the heat exchange between aquifer and adjacent aquitard layers. He developed simplified analytical solutions for advective–diffusive heat transport in an aquifer close to injection wells for transient and periodic conditions. Heat transport in the top and bottom layers is assumed to be vertical and conductive. For a thin aquifer, he adopted Carslaw and Jaeger's (1959) solution for one-dimensional, purely advective heat transport and exchange with adjacent semi-infinite layers. The further assumption for vertical temperature profiles in thin aquifers is referred to as Lauwerier's (1955) assumption. As already shown by Gringarten and Sauty (1975), the approach is also valid for two-dimensional heat transport if heat transport perpendicular to streamlines is neglected. Due to the heat exchange, considerable damping of temperature changes may take place. Uffink (1983) further shows that for periodic boundary conditions, the thickness of the aquifer (typically thicker than a few meters) has to be taken into account for the vertical heat exchange.

Güven et al. (1983) derived analytical expressions for the temperature distribution of a simplified aquifer thermal energy storage concept, taking heat exchange at the soil surface into account. The system is restricted to heat conduction processes in a cylindrical region.

A unified mathematical analysis and analytical solutions of heat and mass diffusion problems were presented by Mikhailov and Özişik (1984) and Häfner et al. (1992).

Bundschuh (1993) formulated analytical models for the simulation of periodic temperature variations in shallow aquifer.

Lu and Ge (1996) developed an analytical solution for the vertical temperature distribution in a semiconfining layer of an aquifer, in order to investigate the effect of horizontal water and heat flow. Their solution is an extension of the one-dimensional approach of Bredehoeft and Papadopulos (1965).

Incropera et al. (2007) describe analytical solutions for a series of technical problems, like heat exchanger systems.

Yang and Yeh (2008) formulated an analytical model for the radial heat transfer during the injection of hot water into a confined aquifer. Heat fluxes in the underlying and overlying rock are restricted to vertical conductive flux. Effects of heat dispersion are neglected.

Woods and Ortega (2011) formulated an analytical model to investigate the thermal response of a line of standing column wells and compared simulation results with results from numerical simulations.

Furthermore, for **borehole heat exchanger** (BHE) systems, various analytical models have been developed in the past. Based on analytical solutions of Eskilson and Claesson (1988) for BHEs and analytical expressions of Hellström (1991) for the thermal resistance of BHEs (Section 2.1.2.6), the **software EED** (Earth Energy Designer, current Version 3.16, BLOCON 2008) for the design of BHEs was developed. The software allows either the calculation of mean fluid temperature in BHEs, which are embedded in a medium with given properties (thermal conductivity, thermal capacity, mean ground surface temperature, geothermal heat flux) for given thermal load and BHE layout (diameter and length of borehole, type of BHE configuration), or the calculation of the required borehole length for given minimum and maximum temperatures of the fluid within the BHE. Further alternative software tools are **GLHEPRO** (current version 4.0, 2007) or **EWS** (Huber 2008, current version 4.0). Based on the cylinder source theory, Nagano et al. (2006) developed a **design and performance prediction tool** for ground-source heat pump systems. Lamarche and Beauchamp (2007) presented an analytical solution for the short-term analysis of BHEs with concentric cylindrical tubes. Based on numerical simulations, they demonstrated that the solution is also a good approximation for the U-tube configuration.

In the following, an **overview of analytical solutions**, relevant for the assessment of the thermal use of shallow groundwater systems, is given. We start with closed systems without local water withdrawal and reinjection, which, contrary to open systems, do not modify the original flow field. Thermal sources of the analytical solutions can be represented by a point source, an infinite line source (ILS), or a finite line source (FLS). These are shown schematically in Figure 3.1a through c. The temperature T is the sum of the ambient temperature without thermal use T_0 and a decrease (or increase) ΔT. The thermal velocity and the thermal diffusion/dispersion coefficient are indicated by an index t.

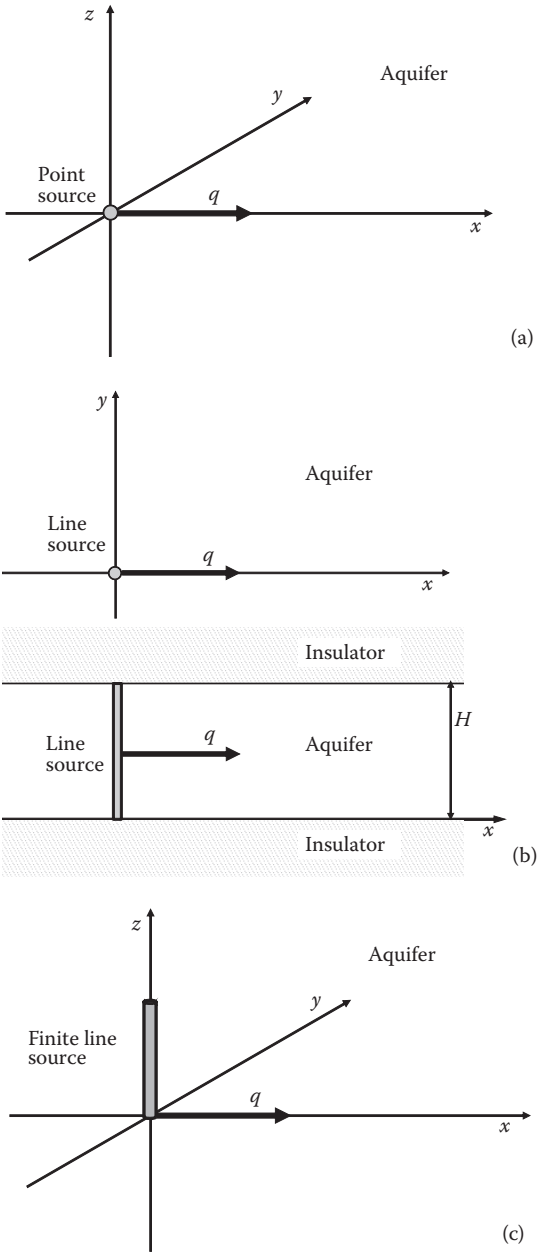

Figure 3.1 Thermal sources. (a) Point source in infinite aquifer with flow field *q*; (b) line source in aquifer layer bound by insulating layers with flow field *q*; (c) FLS in infinite aquifer with flow field *q* (schematic).

3.1 CLOSED SYSTEMS

3.1.1 Instantaneous point source—three-dimensional conduction

The three-dimensional **differential equation for heat conduction** with constant coefficients, and without internal sources or sinks, is

$$\frac{\partial T}{\partial t} = D_t \nabla^2 T = D_t \cdot \left(\frac{\partial^2 T}{\partial x^2} + \frac{\partial^2 T}{\partial y^2} + \frac{\partial^2 T}{\partial z^2} \right) \tag{3.1}$$

where D_t is the thermal diffusion coefficient with $D_t = \lambda_m / C_m$. The initial condition is $T(x, y, z, t = 0) = T_0$. A **quantity of energy** ΔE (J) injected instantaneously at the point (x_0, y_0, z_0) within an infinite three-dimensional aquitard produces a temperature distribution $T(x, y, z, t)$ given by an **instantaneous point source solution** (Carslaw and Jaeger 1959):

$$T(x,y,z,t) = T_0 + \frac{\Delta E}{8C_m(\pi D_t t)^{3/2}} \exp\left[-\frac{(x-x_0)^2 + (y-y_0)^2 + (z-z_0)^2}{4D_t t} \right] \tag{3.2}$$

In each coordinate direction x, y, and z, a bell-shaped temperature distribution is obtained. Accordingly, a negative injection corresponds to heat extraction. The point source may correspond to a small portion of a heat exchanger. Note that the initial temperature at the source location is infinite. This is due to the idealized condition of finite energy in a point.

3.1.2 Moving point source—three-dimensional conduction and advection

The three-dimensional **differential equation for heat conduction and advection** with constant coefficients, without internal sources or sinks, and for uniform groundwater flow in x-direction is

$$\frac{\partial T}{\partial t} = D_{t,L} \frac{\partial^2 T}{\partial x^2} + D_{t,T} \frac{\partial^2 T}{\partial y^2} + D_{t,T} \frac{\partial^2 T}{\partial z^2} - u_{t,x} \frac{\partial T}{\partial x} \tag{3.3}$$

The initial condition is $T(x, y, z, t = 0) = T_0$. The coefficient $D_{t,L}$ (m^2 s^{-1}) includes both thermal diffusion and dispersion. The **moving point source** with source strength $J = dE/dt$ (W) at a point located at (x_0, y_0, z_0) within an infinite three-dimensional aquifer corresponds to the problem of a **point**

source moving in the x-direction in an aquifer with zero flow (Carslaw and Jaeger 1959) with the temperature

$$T(x,y,z,t) = T_0 + \frac{J}{8C_{\mathrm{m}}\left(\pi^3 D_{\mathrm{t,L}} D_{\mathrm{t,T}}^2\right)^{1/2}} \times \int_0^t \exp\left[-\left(\frac{(x - x_0 - u_t \cdot (t - t'))^2}{D_{\mathrm{t,L}}} + \frac{(y - y_0)^2 + (z - z_0)^2}{D_{\mathrm{t,T}}} \right) \frac{1}{4 \cdot (t - t')} \right] \cdot \frac{1}{(t - t')^{3/2}} \mathrm{d}t' \tag{3.4}$$

The evaluation of the integral can be performed numerically. The temperature at the source location is infinite. The continuous point source may correspond to a small portion of a heat exchanger with continuous heat injection/extraction. In this case, the temperature has to be taken at the borehole wall, thus representing an approximation to the real situation.

3.1.3 ILS—two-dimensional conduction

Assuming the BHE as a vertical line source at location (x_0, y_0) with infinite length along the vertical (z_0) direction, we integrate Equation 3.2 along an infinite line, $-\infty < z_0 < \infty$, in order to get the **instantaneous line source** (Carslaw and Jaeger 1959):

$$T(x,y,z,t) = T_0 + \frac{\Delta E/H}{8C_{\mathrm{m}}(\pi D_{\mathrm{t}} t)^{3/2}} \int_{-\infty}^{\infty} \exp\left(-\frac{(x - x_0)^2 + (y - y_0)^2 + (z - z_0)^2}{4 D_{\mathrm{t}} t} \right) \mathrm{d}z_0 \tag{3.5}$$

where $\Delta E/H$ (J m^{-1}) is the heat energy per unit length of the borehole of length H (m), which is extended to the whole infinite length of the borehole of the model. Solving the previous integral results in

$$T(x,y,t) = T_0 + \frac{\Delta E/H}{4\pi\lambda_{\mathrm{m}} t} \exp\left(-\frac{(x - x_0)^2 + (y - y_0)^2}{4 D_{\mathrm{t}} t} \right) \tag{3.6}$$

Integrating Equation 3.6 from $0 < t' < t$, we get the **continuous line source**

$$T(x,y,t) = T_0 + \frac{q_{\mathrm{tb}}}{4\pi\lambda_{\mathrm{m}}} \int_0^t \exp\left(-\frac{r^2}{4 D_{\mathrm{t}} (t - t')} \right) \frac{\mathrm{d}t'}{(t - t')} \tag{3.7}$$

where $q_{tb} = J/H = (dE/dt)/H$ (W m^{-1}) is the **heat flow rate per unit length of the borehole** and $r^2 = (x - x_0)^2 + (y - y_0)^2$ is the radial coordinate. Introducing the dimensionless variable $u = r^2/4D_t(t - t')$ and the term $dt'/(t - t') = du/u$ results in

$$T(x,y,t) = T_0 + \frac{q_{tb}}{4\pi\lambda_m} \int_{r^2/(4D_t t)}^{\infty} \exp(-u)\frac{du}{u} \tag{3.8}$$

Moreover, making use of the definition of the **exponential integral**

$$-\mathrm{Ei}(-x) = \int_x^{\infty} e^{-u}\frac{du}{u} \tag{3.9}$$

the solution for the **ILS** can be expressed as follows:

$$T(x,y,t) = T_0 - \frac{q_{tb}}{4\pi\lambda_m}\mathrm{Ei}\left(-\frac{r^2}{4D_t t}\right) \tag{3.10}$$

In hydrological literature, the function $-\mathrm{Ei}(-x)$ is also known as the well function $W(x)$. Equation 3.10 is, in particular, applicable for the evaluation of short-term geothermal field experiments such as thermal response tests, which usually last from 12 to 60 h (Signorelli et al. 2007). Introducing the **dimensionless temperature rise** $\Theta = 4\pi\lambda_m\Delta T/(J/H)$, where $\Delta T = T - T_0$, the **dimensionless radial coordinate** $R = r/L$, where L is the length scale of interest, and the **Fourier number** Fo, which can be interpreted as dimensionless time, with

$$\mathrm{Fo} = D_t t/L^2 \tag{3.11}$$

we can express Equation 3.10 in dimensionless form as follows:

$$\Theta_{ILS} = -\mathrm{Ei}\left[-\frac{R^2}{4\mathrm{Fo}}\right] \tag{3.12}$$

The instantaneous and the continuous ILS models can be directly applied for a **thin BHE** sufficiently far away from the upper and lower ends of the BHE. Moreover, it can be applied for a **finite soil layer** of thickness H (length of the BHE), which is **limited by a thermally insulating top and bottom layer** (Figure 3.1b).

Based on the infinite line-source model and the thermal load of a BHE system, Michopoulos and Kyriakis (2009) developed and evaluated a model to predict the temperature at the exit of a vertical ground heat exchanger.

The **coded function** (MATLAB script) of the **ILS** model (Equation 3.10) is listed as *T_ILS.m*. It can be found at http://www.crcpress.com/product/isbn/9781466560192. A program to visualize the two-dimensional temperature field response for a single borehole with a continuous heat flow rate is available as *closedsys.m*. As an example, Figure 3.2 shows the radial temperature propagation after 90 days of operating a BHE with specific heat extraction $q_{tb} = J/H$ of 50 W m^{-1}.

Solutions to the ILS model for the **time-dependent heat input function of a group of BHEs** can be obtained by applying the superposition principle over all BHEs and over a series of time increments. Figure 3.3 shows the seasonal heat input defined by a cosine function as

$$J_{BHE}(x = 0, t) = J_{ampl}\cos(\alpha - \omega t) \tag{3.13}$$

for $\alpha = 0$ (phase shift) and the heat input amplitude $J_{ampl} = 62.8$ W m^{-1}. The symbol ω (s^{-1}) is the angular frequency, where $\omega = 2\pi/\tau$ with the length of the period τ.

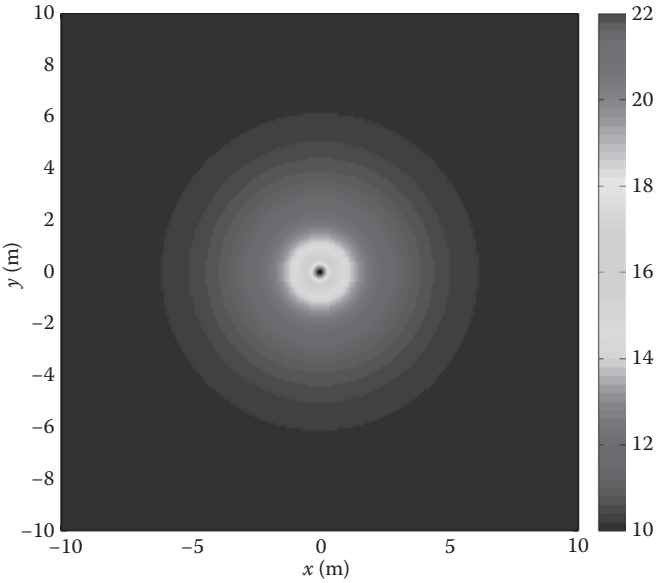

Figure 3.2 **(See color insert.)** Temperature field for a single BHE with constant energy extraction after 90 days. ILS model ($q_{tb} = J/H = 50$ W m^{-1}, $T_0 = 10$°C, $D_t = 9 \times 10^{-7}$ m^2 s^{-1}).

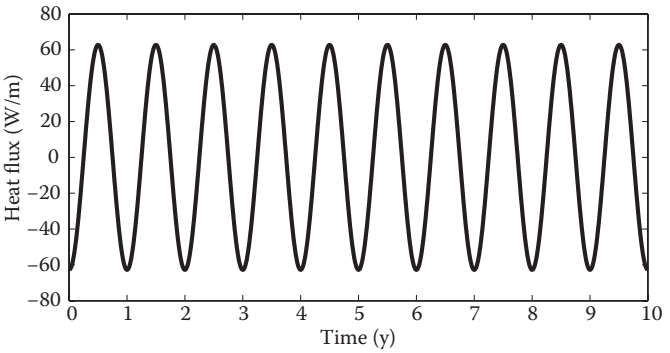

Figure 3.3 Seasonal cosine heat input function (example).

The temperature field of **interacting boreholes** is calculated by summing up the temperature response of individual BHEs:

$$\Delta T = \sum_{i=1}^{N} \Delta T_i \tag{3.14}$$

where N denotes the number of BHEs. A MATLAB program to visualize a two-dimensional temperature field response for multiple boreholes is listed as *closedsys_mBHE.m*. Figure 3.4a through d shows the seasonal heat input and temperature maps for the times 10.0, 10.25, 10.5, and 10.75 years after the operation began. The system has almost reached quasi-steady state. The geometric arrangement and operation mode adjustment in low enthalpy geothermal fields for heating was studied by Beck et al. (2013) using similar models.

3.1.4 Infinite cylindrical source—two-dimensional conduction

For cases in which the **radius of the BHE** (r_0) **is important, the source is considered as a cylindrical surface** and the heat flow rate is applied at $r = r_0$. Ingersoll et al. (1954) presented the following equation:

$$T(x,y,t) = T_0 + \frac{q_{\mathrm{tb}}}{\pi^2 \lambda_{\mathrm{m}}} \int_0^{\infty} \frac{e^{-\beta^2 \mathrm{Fo}} - 1}{\mathrm{J}_1^2(\beta) + \mathrm{Y}_1^2(\beta)} \times [\mathrm{J}_0(R\beta)\mathrm{Y}_1(\beta) - \mathrm{J}_1(\beta)\mathrm{Y}_0(R\beta)] \frac{\mathrm{d}\beta}{\beta^2} \tag{3.15}$$

where $R = r/r_0$ ($L = r_0$) is the dimensionless cylindrical radius. The functions J_0 and J_1 are Bessel functions of the first kind and of orders zero and one, whereas Y_0 and Y_1 are Bessel functions of the second kind of orders zero and one. Equation 3.15 is difficult to evaluate. A simpler expression can be

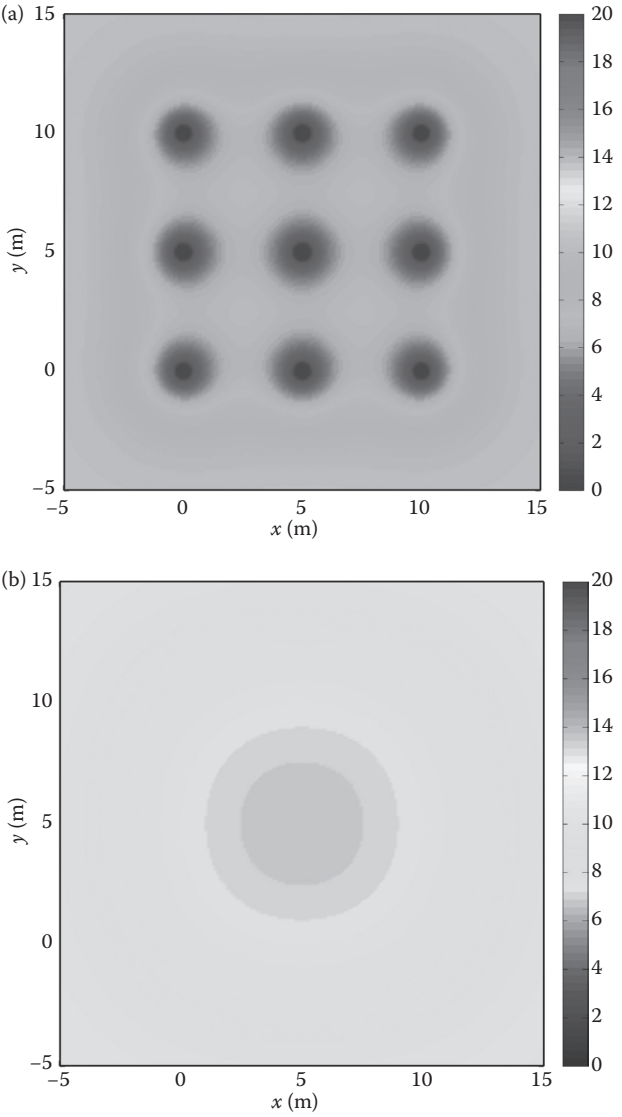

Figure 3.4 **(See color insert.)** Heat exchanger group 3 × 3 calculated with ILS model with seasonal cosine heat input. (a) Map after 10.0 years; (b) 10.25 years; (c) 10.5 years; and (d) 10.75 years.

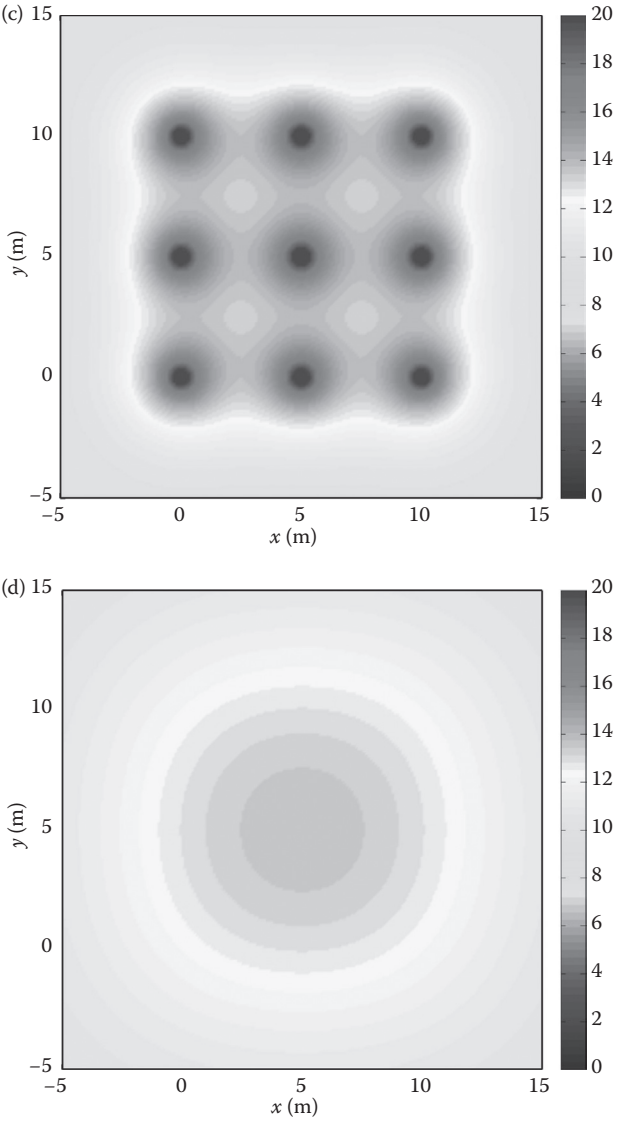

Figure 3.4 (Continued) **(See color insert.)** Heat exchanger group 3 × 3 calculated with ILS model with seasonal cosine heat input. (a) Map after 10.0 years; (b) 10.25 years; (c) 10.5 years; and (d) 10.75 years.

derived by expressing the line source model (Equation 3.10) in radial coordinates (r, φ_r) for a line source at location r_0 and φ'_r:

$$T(r,\varphi,t) = T_0 - \frac{q_{tb}}{4\pi\lambda_m}\,\mathrm{Ei}\left(-\frac{r^2 + r_0^2 - 2rr_0\cos(\varphi_r - \varphi'_r)}{4D_t t}\right) \tag{3.16}$$

where r and φ_r denote the radial and angular coordinates, respectively. Integrating Equation 3.16 around a circle of radius r_0, the **infinite cylindrical source** (ICS) can be expressed as follows (Man et al. 2010):

$$T(r,t) = T_0 - \frac{q_{tb}}{4\pi\lambda_m}\int_0^{\pi}\frac{1}{\pi}\,\mathrm{Ei}\left(-\frac{r^2 + r_0^2 - 2rr_0\cos\varphi'_r}{4D_t t}\right)\mathrm{d}\varphi'_r \tag{3.17}$$

The integral can be evaluated numerically. Introducing the dimensionless time $\mathrm{Fo} = D_t t/r_0^2$ ($L = r_0$), we can express the **dimensionless temperature rise** according to Equation 3.17 in dimensionless form:

$$\Theta_{ICS} = -\frac{1}{\pi}\int_0^{\pi}\mathrm{Ei}\left(-\frac{R^2 + 1 - 2R\cos\varphi'_r}{4\,\mathrm{Fo}}\right)\mathrm{d}\varphi'_r \tag{3.18}$$

Equations 3.17 and 3.18 were first introduced by Man et al. (2010) to simulate heat transfer by pile ground heat exchangers.

Figure 3.5 shows the **difference of the ILS and ICS models**, especially for short time simulations. The ICS model is more suitable for short time simulations compared to the ILS. Figure 3.6 reveals that the effect of assuming the borehole as an ILS becomes irrelevant for $\mathrm{Fo} \geq 8$ ($L = r_0$) when $R = 1$ (at the borehole wall) assuming $\Theta_{ILS}/\Theta_{ICS} > 0.99$ as a criterion. Eskilson (1987) states that the ILS model is valid for $\mathrm{Fo} > 5$. In comparison, Ingersoll et al. (1954) were more strict and stated that the ILS model is only valid for $\mathrm{Fo} > 20$. Philippe et al. (2009) investigated the validity range of analytical solutions to the ILS, FLS, and ICS models. Bernier et al. (2004) suggested a technique to aggregate heating and cooling loads when using the cylindrical source models to perform annual hourly energy simulations of ground coupled heat pump systems.

The **coded function** (MATLAB script) of the **ICS** model (Equation 3.17) is available as *T_ICS.m*. As an example, a BHE with specific heat extraction $q_{tb} = J/H$ of 50 W m^{-1} and a radius of 0.1 m in an aquifer with a thermal

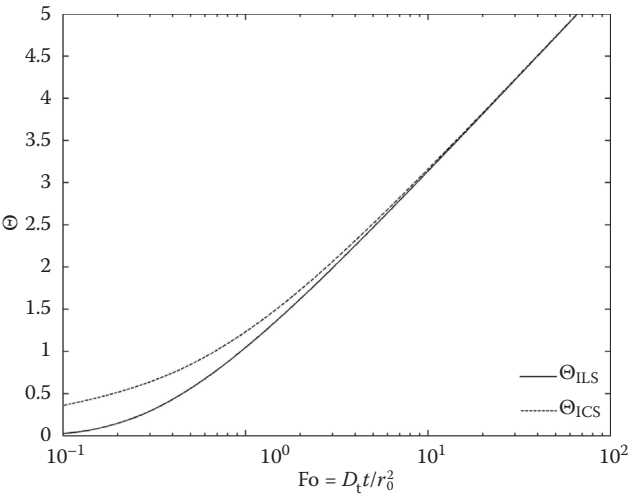

Figure 3.5 Dimensionless temperature as function of dimensionless time Fo (R = 1.0, $L = r_0$).

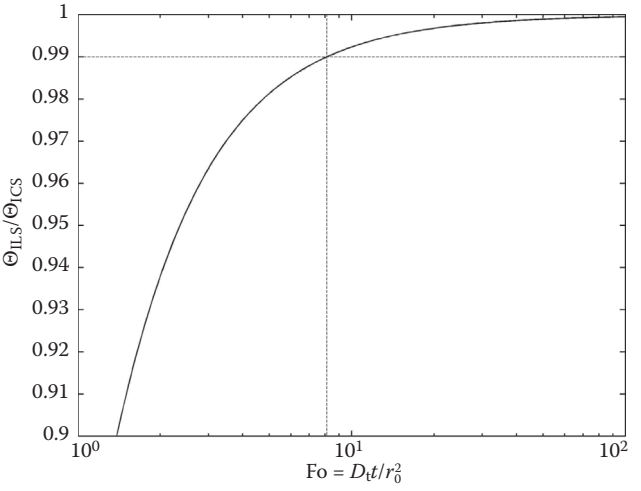

Figure 3.6 Ratio of ILS and ICS models over the dimensionless time Fo (R = 1.0, $L = r_0$).

diffusion coefficient of 9.0×10^{-7} m^2 s^{-1} results in a temperature change at the borehole wall of –1.6 K after 3 h (Fo = 1.0) when using the ILS model. In comparison, the ICS yields a temperature change of –1.9 K. Due to this discrepancy, the use of the more appropriate ICS is favorable for these specific conditions.

3.1.5 FLS—three-dimensional conduction

In order to account for axial effects, the borehole must be considered to have finite length. Integrating Equation 3.2 between $0 \le t' \le t$, we get the **continuous point source** (Carslaw and Jaeger 1959):

$$T(r,t) = T_0 + \frac{J}{8C_m \cdot (\pi D_t)^{3/2}} \int_0^t \exp\left(\frac{r'^2}{4D_t \cdot (t-t')}\right) \frac{dt'}{(t-t')^{3/2}} \tag{3.19}$$

where $J = dE/dt$ (W) is the strength of the continuous point source and

$$r' = \sqrt{(x-x_0)^2 + (y-y_0)^2 + (z-z_0)^2} = \sqrt{r^2 + (z-z_0)^2} \tag{3.20}$$

is the radial coordinate. Applying the change of variables $\tau = (t - t')^{-1/2}$ and $dt'/(t - t')^{-3/2} = 2d\tau$ results in

$$T(r,t) = T_0 + \frac{J}{4C_m(\pi D_t)^{3/2}} \int_{1/\sqrt{t}}^{\infty} \exp\left(-\frac{r'^2\tau^2}{4D_t}\right) d\tau \tag{3.21}$$

and finally in

$$T(x,y,z,t) = T_0 + \frac{J}{4\pi\lambda_m r'} \operatorname{erfc}\left(\frac{r'}{\sqrt{4D_t t}}\right) \tag{3.22}$$

where erfc(x) is the **complementary error function:**

$$\operatorname{erfc}(x) = \frac{2}{\sqrt{\pi}} \int_x^{\infty} \exp(-y^2)\, dy \tag{3.23}$$

When t approaches infinity, Equation 3.22 can be approximated by the **steady-state point source solution:**

$$T(x,y,z) = T_0 + \frac{J}{4\pi\lambda_m r'} \tag{3.24}$$

The contributions of point sources of equal energy injection/extraction making up a line source can be added (Eskilson 1987; Lamarche and Beauchamp 2007; Marcotte et al. 2010; Zeng et al. 2002), and the constant surface temperature boundary condition can be satisfied by applying the

method of images (Figure 3.7). Applying this method (Eskilson 1987; Zeng et al. 2002) to Equation 3.22 yields the **FLS** model:

$$T(x,y,z,t) = T_0 + \frac{q_{tb}}{4\pi\lambda_m}\left\{\int_0^H \frac{\operatorname{erfc}\left(r'/\sqrt{4D_t t}\right)}{r'}\mathrm{d}z_0 - \int_{-H}^0 \frac{\operatorname{erfc}\left(r'/\sqrt{4D_t t}\right)}{r'}\mathrm{d}z_0\right\} \tag{3.25}$$

where H is the borehole length.

For **steady-state conditions**, Equation 3.25 reduces to

$$T(x,y,z) = T_0 + \frac{q_{tb}}{4\pi\lambda_m}\ln\left(\frac{H-z+\sqrt{r^2+(H-z)^2}}{H+z+\sqrt{r^2+(H+z)^2}}\cdot\frac{2z^2+2z\sqrt{r^2+z^2}+r^2}{r^2}\right) \tag{3.26}$$

Introducing the dimensionless time $\mathrm{Fo} = D_t t/H^2$ ($L = H$) and the dimensionless coordinates $R = r/H$, $Z = z/H$, and $Z' = z_0/H$, we can express the transient FLS model (Equation 3.25) **in dimensionless form:**

$$\Theta_{FLS} = \int_0^1 \frac{\operatorname{erfc}\left[\sqrt{R^2+(Z-Z')^2}\,/\,2\sqrt{\mathrm{Fo}}\right]}{\sqrt{R^2+(Z-Z')^2}}\mathrm{d}Z' - \int_{-1}^0 \frac{\operatorname{erfc}\left[\sqrt{R^2+(Z-Z')^2}\,/\,2\sqrt{\mathrm{Fo}}\right]}{\sqrt{R^2+(Z-Z')^2}}\mathrm{d}Z' \tag{3.27}$$

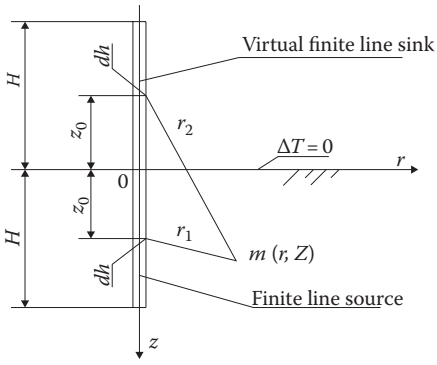

Figure 3.7 Representation of the FLS. (Modified after Zeng, H.Y. et al. *Heat Transfer-Asian Research* 31 (7), 558–567, 2002.)

and also the steady-state Equation 3.26:

$$\Theta_{\text{FLS\_steady-state}} = \ln\left[\frac{1-Z+\sqrt{R^2+(1-Z)^2}}{1+Z+\sqrt{R^2+(1+Z)^2}} \cdot \frac{2Z^2+2Z\sqrt{R^2+Z^2}+R^2}{R^2}\right] \quad (3.28)$$

From Figure 3.8, it can be seen that **axial effects become important for long time simulations**. The shorter the borehole length, the higher the discrepancy between the ILS and FLS models. Figure 3.9 shows that the axial effects are negligible for Fo < 0.052 ($L = H$) when $R = 0.005$ ($H = 10$ m, $r = r_0 = 0.05$ m) assuming $\Theta_{FLS}/\Theta_{ILS} > 0.9$ as a criterion. For $R = 0.0005$ ($H = 100$ m, $r = r_0 = 0.05$ m), axial effects are negligible for Fo < 0.065. Eskilson (1987) is more restrictive and states that the ILS model is valid for Fo < 0.01.

Bandos et al. (2009) present a solution to the FLS model, which takes into account the prevailing geothermal gradient and arbitrary ground surface temperatures. Marcotte et al. (2010) investigated the importance of axial effects by comparing solutions of the ILS and FLS models. Cui et al. (2006) formulated an inclined FLS analytical solution.

The **coded functions** (MATLAB scripts) of the **FLS** model for transient (Equation 3.25) and steady-state conditions (Equation 3.26) are listed as

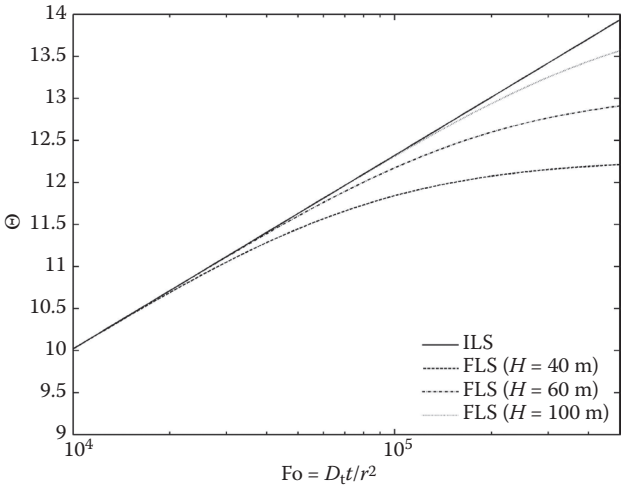

Figure 3.8 Dimensionless temperature response at the borehole wall over dimensionless time for different borehole lengths H (m) ($R = 0.005$, $L = H = 10$ m, $r = r_0 = 0.05$ m, $z = 0.5 \times H$).

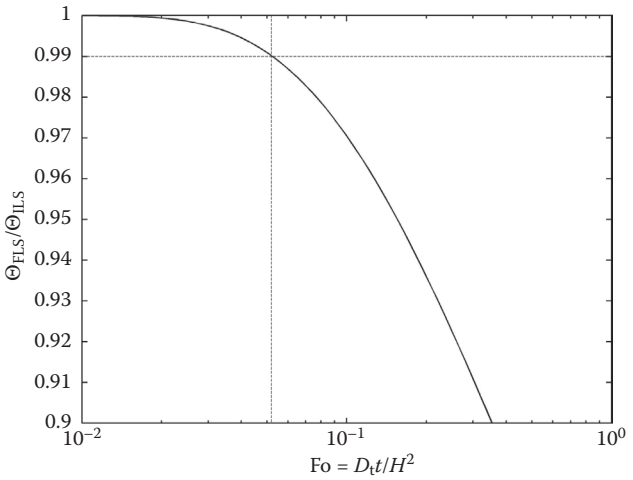

Figure 3.9 Ratio of the FLS and the ILS models over the dimensionless time Fo (R = 0.005, $L = H$ = 10 m, r = 0.05 m, $z = 0.5 \times H$).

T_FLS.m and *T_FLSs.m*, respectively. A program to visualize the temperature at the borehole wall over time for a single borehole with a continuous heat flow rate is listed as *closedsys_Tb.m*. As an example, Figure 3.10 shows the temperature response at the borehole wall for a BHE with specific heat extraction $q_{tb} = J/H$ of 50 W m^{-1} using the ILS and FLS models.

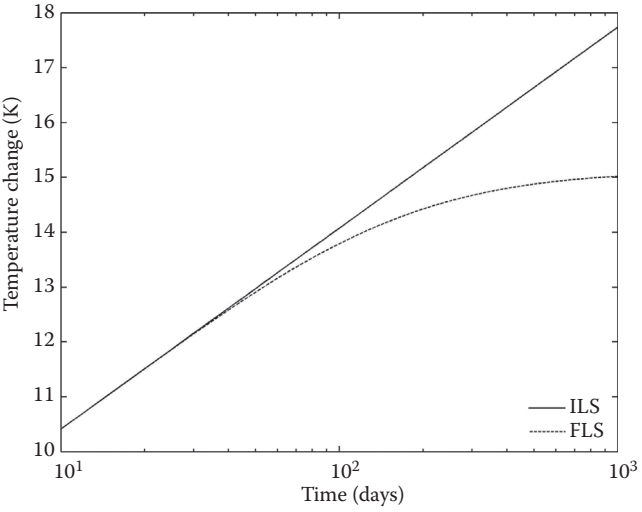

Figure 3.10 Temperature response at the borehole wall over time (H = 10 m, $z = 0.5 \times H$, $D_t = 9 \times 10^{-7}$ m^2 s^{-1}).

3.1.6 Finite cylindrical source—three-dimensional conduction

First, we express the **continuous point source model** (Equation 3.22) in radial coordinates as follows:

$$T(r,\varphi_{r^3},z,t)=T_0+\frac{J}{4\pi\lambda_{\mathrm{m}}}\frac{\operatorname{erfc}\left(\sqrt{r^2+r_0^2-2rr_0\cos(\varphi_r-\varphi'_r)+(z-z_0)^2}\Big/\sqrt{4D_{\mathrm{t}}t}\right)}{\sqrt{r^2+r_0^2-2rr_0\cos(\varphi_r-\varphi'_r)+(z-z_0)^2}} \tag{3.29}$$

Then we integrate Equation 3.29 around a circle of radius r_0 in order to get the **continuous ring source** model:

$$T(r,z,t)=T_0+\frac{J}{4\pi\lambda_{\mathrm{m}}}\int_0^{\pi}\frac{\operatorname{erfc}\left[\sqrt{r^2+r_0^2-2rr_0\cos\varphi'_r+(z-z_0)^2}\Big/\sqrt{4D_{\mathrm{t}}t}\right]}{\pi\sqrt{r^2+r_0^2-2rr_0\cos\varphi'_r+(z-z_0)^2}}\,\mathrm{d}\varphi'_r \tag{3.30}$$

For **steady-state conditions**, Equation 3.30 reduces to

$$T(r,z)=T_0+\frac{J}{4\pi\lambda_{\mathrm{m}}}\int_0^{\pi}\frac{1}{\pi\sqrt{r^2+r_0^2-2rr_0\cos\varphi'_r+(z-z_0)^2}}\,\varphi'_r \tag{3.31}$$

Integrating over the borehole length and adding the upper constant temperature boundary condition by applying the method of images to Equations 3.30 and 3.31 yields the **finite cylindrical source** (FCS) model:

$$T(r,z,t)=T_0+\frac{q_{\mathrm{tb}}}{4\pi\lambda_{\mathrm{m}}}\left\{\int_0^H\int_0^{\pi}\frac{\operatorname{erfc}\left[r'\Big/\sqrt{4D_{\mathrm{t}}t}\right]}{\pi r'}\mathrm{d}\varphi'_r\,\mathrm{d}z'-\int_{-H}^0\int_0^{\pi}\frac{\operatorname{erfc}\left[r'\Big/\sqrt{4D_{\mathrm{t}}t}\right]}{\pi r'}\mathrm{d}\varphi'_r\,\mathrm{d}z'\right\} \tag{3.32}$$

$$T(r,z)=T_0+\frac{q_{\mathrm{tb}}}{4\pi\lambda_{\mathrm{m}}}\left\{\int_0^H\int_0^{\pi}\frac{1}{\pi r'}\mathrm{d}\varphi'_r\,\mathrm{d}z'-\int_{-H}^0\int_0^{\pi}\frac{1}{\pi r'}\mathrm{d}\varphi'_r\,\mathrm{d}z'\right\} \tag{3.33}$$

where $r' = \sqrt{r^2 + r_0^2 - 2rr_0\cos\varphi_r' + (z - z')^2}$. Similar equations have been presented by Man et al. (2010). Expressing Equations 3.32 and 3.33 **in dimensionless form** yields

$$\Theta_{\mathrm{FCS}} = \int_0^1 \int_0^{\pi} \frac{\operatorname{erfc}\left[R'/2\sqrt{\mathrm{Fo}}\right]}{\pi R'} \mathrm{d}\varphi_r' \, \mathrm{d}Z' - \int_{-1}^0 \int_0^{\pi} \frac{\operatorname{erfc}\left[R'/2\sqrt{\mathrm{Fo}}\right]}{\pi R'} \mathrm{d}\varphi_r' \, \mathrm{d}Z' \quad (3.34)$$

$$\Theta_{\mathrm{FCS\_steady\text{-}state}} = \int_0^1 \int_0^{\pi} \frac{1}{\pi R'} \mathrm{d}\varphi_r' \, \mathrm{d}z' - \int_{-1}^0 \int_0^{\pi} \frac{1}{\pi R'} \mathrm{d}\varphi_r' \, \mathrm{d}z' \quad (3.35)$$

where $R' = \sqrt{R^2 + R_0^2 - 2RR_0\cos\varphi_r' + (Z - Z')^2}$ and $R_0 = r_0/L$.

The behavior with respect to the influence of the borehole radius in a conduction-dominated problem is similar to the one shown in Figures 3.5 and 3.6.

The **coded functions** (MATLAB script) of the **FCS** model for transient (Equation 3.32) and steady-state (Equation 3.33) conditions are listed as *T_FCS.m* and *T_FCSs.m*, respectively.

3.1.7 Moving ILS—two-dimensional conduction and advection

An ILS in an aquifer with uniform flow according to Figure 3.1b corresponds to the moving ILS (MILS). Applying the moving source theory to Equation 3.7 yields the analytical solution for the response of a constant line source of infinite length along the vertical direction with a continuous heat flow rate $q_{\mathrm{tb}} = J/H$ per unit length of the borehole, or the **MILS model**:

$$T(x,y,t) = T_0 + \frac{q_{\mathrm{tb}}}{4\pi\lambda_{\mathrm{m}}} \int_0^t \exp\left(-\frac{\{(x - u_{\mathrm{t}} \cdot (t - t')\}^2 + y^2}{4D_{\mathrm{t}} \cdot (t - t')} \right) \frac{\mathrm{d}t'}{(t - t')} \quad (3.36)$$

For the sake of simplicity, the source is located at $x_0 = y_0 = 0$. Applying the following change of variable $\psi = r^2/4D_{\mathrm{t}} \cdot (t - t')$, $\mathrm{d}t'/(t - t') = \mathrm{d}\psi/\psi$, and $r = \sqrt{x^2 + y^2}$ yields

$$T(x,y,t) = T_0 + \frac{q_{\mathrm{tb}}}{4\pi\lambda_{\mathrm{m}}} \exp\left[\frac{u_{\mathrm{t}} x}{2D_{\mathrm{t}}} \right] \int_{r^2/4D_{\mathrm{t}}t}^{\infty} \exp\left[-\psi - \frac{u_{\mathrm{t}}^2 r^2}{16 D_{\mathrm{t}}^2 \psi} \right] \frac{\mathrm{d}\psi}{\psi} \quad (3.37)$$

For **steady state-conditions,** Equation 3.37 becomes (Carslaw and Jaeger 1959)

$$T(x,y) = T_0 + \frac{q_{\mathrm{tb}}}{2\pi\lambda_{\mathrm{m}}} \exp\left[\frac{u_{\mathrm{t}}x}{2D_{\mathrm{t}}}\right] \mathrm{K}_0\left[\frac{u_{\mathrm{t}}\sqrt{x^2+y^2}}{2D_{\mathrm{t}}}\right] \tag{3.38}$$

in which K_0 is the modified Bessel function of the second kind of order zero. Equations 3.37 and 3.38 have previously been used by Sutton et al. (2003), Zubair and Chaudhry (1996), and Diao et al. (2004) to calculate the ground resistance, temperature distributions for time-dependent energy extraction/injection, and the effects of groundwater advection on ground-source heat pump systems.

Introducing the thermal Peclet number $\mathrm{Pe} = u_t L/D_t$, we can express the **MILS model** (Equation 3.37) **in dimensionless form** as follows:

$$\Theta_{\mathrm{MILS}} = \exp\left[\frac{\mathrm{Pe}}{2} R\cos\varphi_r\right] \int_{R^2/4\mathrm{Fo}}^{\infty} \exp\left[-\psi - \frac{\mathrm{Pe}^2 R^2}{16\psi}\right] \frac{\mathrm{d}\psi}{\psi} \tag{3.39}$$

$$\Theta_{\mathrm{MILS\_steady\text{-}state}} = 2\exp\left[\frac{\mathrm{Pe}}{2} R\cos\varphi_{\mathrm{r}}\right] \mathrm{K}_0\left[\frac{\mathrm{Pe}}{2} R\right] \tag{3.40}$$

Recall that φ_r is the angular coordinate (polar angle) and $R = r/L$. If groundwater flow is present, temperature distribution in the x–y plane is not symmetrical with respect to the polar angle. Figure 3.11 shows the dimensionless temperature distribution using Equation 3.40.

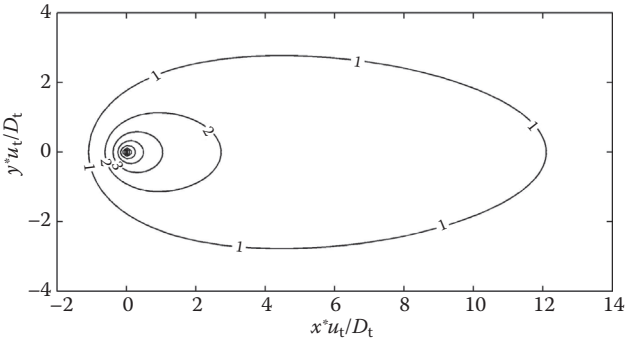

Figure 3.11 Steady-state dimensionless isotherms considering background groundwater flow (q = 1.0 × 10^{-6} m s^{-1}, D_t = 9 × 10^{-7} m^2 s^{-1}).

The **coded functions** (MATLAB script) of the **MILS** model for transient (Equation 3.37) and steady-state (Equation 3.38) conditions are listed as *T_MILS.m* and *T_MILSs.m*, respectively. A program to visualize the two-dimensional temperature field response for a single borehole with continuous heat flow rate in an aquifer with uniform horizontal groundwater flow is listed as *closedsys.m*. As an example, Figure 3.12 shows the two-dimensional temperature response for steady-state conditions of a BHE with specific heat extraction $q_{tb} = J/H$ of 50 W m^{-1}. The aquifer has an initial temperature $T_0 = 10$°C, a thermal diffusion coefficient of 9×10^{-7} m^2 s^{-1}, and a uniform groundwater flow velocity of 1.0×10^{-6} m s^{-1}. An example of a two-dimensional temperature field of multiple BHEs in an aquifer with background groundwater flow is shown in Figure 3.13. The **program** is listed as *closedsys_mBHE.m*.

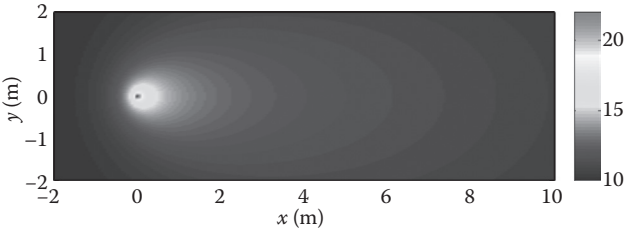

Figure 3.12 **(See color insert.)** Temperature field for a single BHE with constant energy extraction after 90 days ($q_{tb} = J/H = 50$ W m^{-1}, $T_0 = 10$°C, $q = 1.0 \times 10^{-6}$ m s^{-1}, $D_t = 9 \times 10^{-7}$ m^2 s^{-1}).

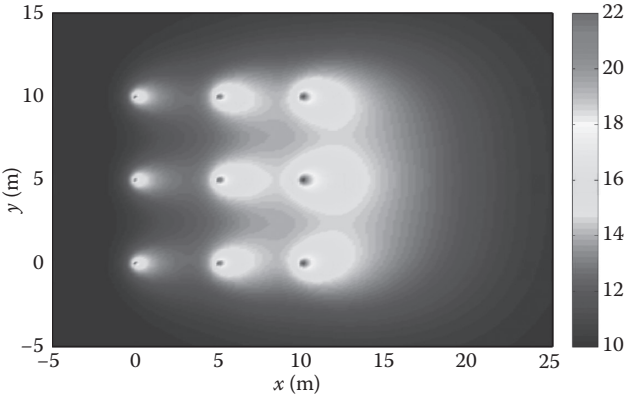

Figure 3.13 **(See color insert.)** Temperature field of multiple interacting BHEs with constant energy extraction after 90 days ($q_{tb} = J/H = 50$ W m^{-1}, $T_0 = 10$°C, $q = 1.0 \times 10^{-6}$ m s^{-1}, $D_t = 9 \times 10^{-7}$ m^2 s^{-1}).

In order to compute the mean temperature around a borehole in an aquifer with uniform horizontal groundwater flow, the integral average of the temperature response of a circle of radius r_0 must be estimated (Diao et al. 2004).

Taking into account the following definition of the modified Bessel function of the first kind and of order zero

$$\mathrm{I}_0(u) = \frac{1}{\pi}\int_0^{\pi} \exp(u\cos\varphi')\,\mathrm{d}\varphi' \tag{3.41}$$

the mean temperature at the borehole wall ($r = r_0$) for the **MILS** for transient (Equation 3.37) and steady-state conditions (Equation 3.38) is as follows:

$$T(r_0,t) = T_0 + \frac{q_{\mathrm{tb}}}{4\pi\lambda_{\mathrm{m}}}\mathrm{I}_0\left[\frac{u_{\mathrm{t}}r}{2D_{\mathrm{t}}}\right]\int_{r^2/4D_{\mathrm{t}}t}^{\infty}\exp\left[-\psi - \frac{u_{\mathrm{t}}^2r^2}{16D_{\mathrm{t}}^2\psi}\right]\frac{\mathrm{d}\psi}{\psi} \tag{3.42}$$

$$T(r_0) = T_0 + \frac{q_{\mathrm{tb}}}{2\pi\lambda_{\mathrm{m}}}\mathrm{I}_0\left[\frac{u_{\mathrm{t}}r}{2D_{\mathrm{t}}}\right]\mathrm{K}_0\left[\frac{u_{\mathrm{t}}r}{2D_{\mathrm{t}}}\right] \tag{3.43}$$

In dimensionless form, we get

$$\Theta_{\mathrm{MILS}} = \mathrm{I}_0\left[\frac{\mathrm{Pe}}{2}R\right]\int_{R^2/4\mathrm{Fo}}^{\infty}\exp\left[-\psi - \frac{\mathrm{Pe}^2R^2}{16\psi}\right]\frac{\mathrm{d}\psi}{\psi} \tag{3.44}$$

$$\Theta_{\mathrm{MILS\_steady\text{-}state}} = 2\,\mathrm{I}_0\left[\frac{\mathrm{Pe}}{2}R_0\right]\mathrm{K}_0\left[\frac{\mathrm{Pe}}{2}R_0\right] \tag{3.45}$$

Although a BHE consists of a buried pipe, which commonly is embedded in grouting material, the approximation by a line source is commonly accepted as an approximation in heat transport models of ground-source systems (Diao et al. 2004; Eskilson 1987; Sutton et al. 2003).

The **coded functions** (MATLAB script) of the **MILS** model for computing the mean temperature at the borehole wall (Equations 3.42 and 3.43) are *T_MILSc.m* and *T_MILScs.m*, respectively. An example of the

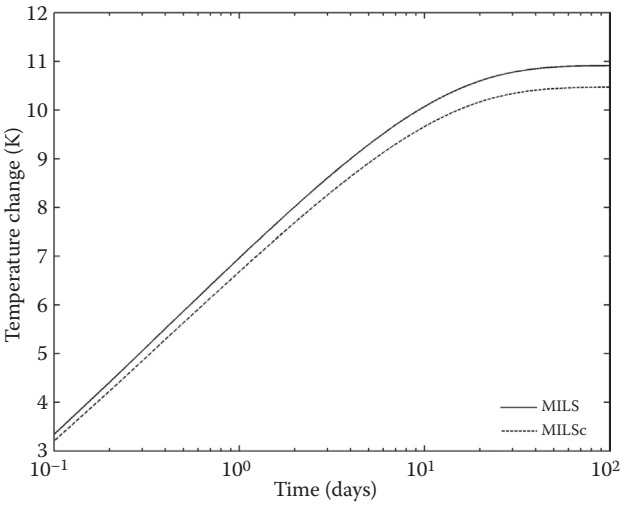

Figure 3.14 Temperature response at the borehole wall over time ($q_{tb} = J/H = 50$ W m^{-1}, $q = 1.0 \times 10^{-6}$ m s^{-1}, $D_t = 9 \times 10^{-7}$ m^2 s^{-1}). MILS: moving ILS ($x = r_0$); MILSc: MILS with mean temperature at the borehole wall ($r = r_0$).

temperature response at the borehole wall is shown in Figure 3.14 using Equations 3.37 and 3.42 with constant energy extraction. Note that in Figure 3.14, Equation 3.42 computes the average temperature around the borehole wall, whereas Equation 3.37 computes the temperature at $x = r_0$ and $y = 0$.

In order to **consider thermal dispersion**, we express the **instantaneous line source** equation (Equation 3.6) for **anisotropic material** (Carslaw and Jaeger 1959) and apply the moving source theory, which yields

$$T(x,y,t) = T_0 + \frac{\Delta E/H}{4\pi C_m \sqrt{D_{t,L} D_{t,T}}\, t} \exp\left[-\frac{[x - u_t t]^2}{4 D_{t,L} t} - \frac{y^2}{4 D_{t,T} t} \right] \tag{3.46}$$

where $D_{t,L}$ and $D_{t,T}$ are the longitudinal and transversal thermal diffusivity coefficients (Equation 2.93), respectively, which include thermal dispersion effects, given by

$$D_{t,L} = D_t + \beta_L u_t \tag{3.47}$$

$$D_{t,T} = D_t + \beta_T u_t \tag{3.48}$$

Let us now consider a continuous line source, where a constant heat flow rate $q_{tb} = J/H$ is continuously injected/extracted. Integrating Equation 3.46 over the time interval $(0, t)$:

$$T(x,y,t) = T_0 + \frac{q_{tb}}{4\pi C_m \sqrt{D_{t,L} D_{t,T}}} \int_0^t \exp\left[\frac{-[x - u_t \cdot (t-t')]^2}{4D_{t,L} \cdot (t-t')} - \frac{y^2}{4D_{t,T} \cdot (t-t')} \right] \times \frac{dt'}{(t-t')} \tag{3.49}$$

and applying the change of variable yields

$$T(x,y,t) = T_0 + \frac{q_{tb}}{4\pi C_m \sqrt{D_{t,L} D_{t,T}}} \exp\left[\frac{u_t x}{2D_{t,L}} \right] \times \int_{\left(\frac{x^2}{4D_{t,L} t} + \frac{y^2}{4D_{t,T} t} \right)}^{\infty} \exp\left[-\psi - \left(\frac{x^2}{D_{t,L}} + \frac{y^2}{D_{t,T}} \right) \frac{u_t^2}{16 D_{t,L} \psi} \right] \frac{d\psi}{\psi} \tag{3.50}$$

Metzger et al. (2004) used this analytical solution to estimate thermal dispersion coefficients for a packed bed of glass spheres. Hecht-Méndez et al. (2013) applied superposition of Equation 3.50 to optimize multiple BHE operation in a BHE field

$$T(x,y) = T_0 + \frac{J/H}{2\pi C_m \sqrt{D_{t,L} D_{t,T}}} \exp\left[\frac{u_t x}{2D_{t,L}} \right] K_0 \left[\frac{u_t}{2} \sqrt{\frac{D_{t,T} x^2 + D_{t,L} y^2}{D_{t,L}^2 D_{t,T}}} \right] \tag{3.51}$$

In Equations 3.49 and 3.50, thermal dispersivities are set to zero ($\beta_L = \beta_T = 0$) when thermal dispersion is ignored. This yields the analytical solutions given by Equations 3.37 and 3.38.

The **coded functions** (MATLAB scripts) of the **MILS** model for transient (Equation 3.35) and steady-state (Equation 3.36) conditions, considering thermal dispersion, are listed as *T_MILSd.m* and *T_MILSsd.m*, respectively.

As an example, Figure 3.15 shows the two-dimensional temperature field response of a BHE with specific heat extraction of 50 W m^{-1} for different values of thermal dispersivity. The length of a plume is defined via an isothermal contour ΔT, as the distance between the source and the intersection of this isothermal contour with the x-axis. Increase in dispersivity

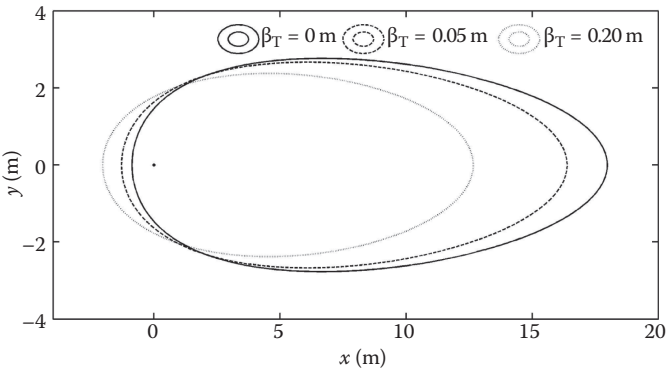

Figure 3.15 Steady-state temperature field for a single BHE with constant energy extraction for different thermal dispersivities (ΔT = 1 K, $q_{tb} = J/H$ = 50 W m^{-1}, q = 1.0 × 10^{-6} m s^{-1}, D_t = 9 × 10^{-7} m^2 s^{-1}). (Modified after Molina-Giraldo, N. et al. *International Journal of Thermal Sciences* 50 (7), 1223–1231, 2011.)

yields shorter temperature plumes for the given ΔT. The relative sensitivity of the temperature change near a BHE to longitudinal dispersivity almost disappears for long-term simulation. In contrast, according to Equation 3.51, sensitivity to transverse dispersivity grows with simulated time.

For steady-state conditions, an approximation can be made in order to calculate the **length of the temperature plume** by using an approximation of the modified Bessel function of the second kind of order zero, $K_0(u)$ (Carslaw and Jaeger 1959):

$$u^{0.5}\exp(u)K_0(u) \approx \sqrt{\frac{\pi}{2}}\left(1-\frac{1}{8u}\right) \tag{3.52}$$

where u is the argument of the Bessel function. Substituting Equation 3.52 into Equation 3.51 and solving for **the temperature plume length** (L_p) yields

$$L_p = \left(\frac{(J/H)^2}{8\pi(C_m)^2 D_{t,T} u_t \Delta T^2}\right)\left(1 \pm \sqrt{1-\frac{8\pi\cdot(C_m)^2 D_{t,L} D_{t,T} \Delta T^2}{(J/H)^2}}\right) \tag{3.53}$$

where ΔT is the value of the isothermal contour. Equation 3.53 has been previously used by Molina-Giraldo et al. (2011a) to evaluate the effect of thermal dispersion in temperature plumes from vertical ground-source heat pump systems. Ham et al. (2004) used it to estimate the effect of dispersion on solute transport.

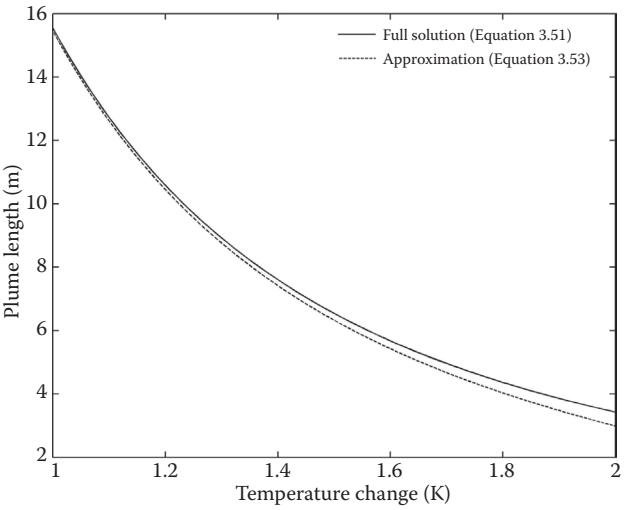

Figure 3.16 Plume length for steady-state conditions as a function of temperature change (q = 1 × 10^{-6} m s^{-1}, D_t = 9 × 10^{-7} m^2 s^{-1}, β_L = 1.0 m, β_T = 0.1 m, $q_{tb} = J/H$ = −50 W m^{-1}, y = 0 m). (Modified after Molina-Giraldo, N. et al. *International Journal of Thermal Sciences* 50 (7), 1223–1231, 2011.)

The **coded function** (MATLAB script) of the **MILS** model to compute the length of the temperature plume at steady-state conditions (Equation 3.53) is available as *T_PL.m*.

Equation 3.53 can be employed to compute the length of a temperature plume (L_p) for a given isothermal contour (ΔT) under steady-state conditions. This is an estimate, which is valid only for $u \gg 1$. According to Abramowitz and Stegun (1964), the relative error of this approximation is around 0.01 when $u > 3$. Figure 3.16 shows an exemplary comparison of the full solution (Equation 3.50) with the approximation (Equation 3.53). The relative error for this specific example is about 8% for a ΔT = 2 K.

3.1.8 Moving FLS—three-dimensional conduction and advection

The temperature response at a given time t due to an energy flux J extracted/injected by a **continuous point source** after applying the moving source theory to Equation 3.2 (Carslaw and Jaeger 1959) is

$$T(x,y,z,t) = T_0 + \frac{J}{8C_m \cdot (\pi D_t)^{3/2}} \int_0^t \exp\left[-\frac{\{(x - u_t \cdot (t-t')\}^2 + y^2 + z^2}{4D_t \cdot (t-t')}\right] \frac{dt'}{(t-t')^{3/2}} \tag{3.54}$$

For the sake of simplicity, the source is located at $x_0 = y_0 = 0$. Applying the change of variable, $\psi = r'/2\sqrt{D_t \cdot (t-t')}$ and $dt'/(t-t')^{3/2} = 4\sqrt{D_t}/r' d\psi$, yields the moving point source equation for a continuous injection:

$$T(x,y,z,t) = T_0 + \frac{J}{2\pi^{3/2}\lambda_m r'} \exp\left[\frac{u_t x}{2D_t}\right] \int_{r'/\sqrt{4D_t t}}^{\infty} \exp\left[-\psi^2 - \frac{u_t^2 r'^2}{16 D_t^2 \psi^2}\right] d\psi \tag{3.55}$$

where $r' = \sqrt{x^2 + y^2 + (z-z_0)^2} = \sqrt{r^2 + (z-z_0)^2}$. For steady-state conditions, Equation 3.55 becomes

$$T(x,y,z,t) = T_0 + \frac{J}{4\pi\lambda_m r'} \exp\left[-\frac{u_t \cdot (r'-x)}{2D_t}\right] \tag{3.56}$$

Applying the following change of variable, $\phi = \psi^2$, to Equation 3.55 yields

$$T(x,y,z,t) = T_0 + \frac{J}{4\pi^{3/2}\lambda_m r'} \exp\left[\frac{u_t x}{2D_t}\right] \int_{r'^2/4D_t t}^{\infty} \exp\left[-\phi - \frac{u_t^2 r'^2}{16 D_t^2 \phi}\right] \frac{d\phi}{\sqrt{\phi}} \tag{3.57}$$

The integral of Equation 3.57 can be expressed as the generalized incomplete Gamma function (Chaudhry and Zubair 1994):

$$\Gamma(1/2, u_1; u_2) = \int_{u_1}^{\infty} \frac{1}{\sqrt{\phi}} \exp\left[-\phi - \frac{u_2}{\phi}\right] d\phi; \quad u_1 = \frac{r'^2}{4D_t t}; \quad u_2 = \frac{u_t^2 r'^2}{16 D_t^2} \tag{3.58}$$

From Equations 3.57 and 3.58, we have the following equation:

$$T(x,y,z,t) = T_0 + \frac{J}{4\pi^{3/2}\lambda_m} \exp\left[\frac{u_t x}{2D_t}\right] \frac{\Gamma(1/2, u_1, u_2)}{r'} \tag{3.59}$$

In order to account for axial effects and constant ground surface temperature conditions, the method of images (Carslaw and Jaeger 1959; Eskilson

1987) is applied to Equation 3.59, resulting in the **moving FLS** (MFLS) model:

$$T(x,y,z,t) = T_0 + \frac{J/H}{4\pi\lambda_m}\exp\left[\frac{u_t x}{2D_t}\right]\left\{\int_0^H \frac{\Gamma(1/2,u_1;u_2)}{\sqrt{\pi}r'}\mathrm{d}z_0 - \int_{-H}^0 \frac{\Gamma(1/2,u_1;u_2)}{\sqrt{\pi}r'}\mathrm{d}z_0\right\} \tag{3.60}$$

The generalized incomplete Gamma function can be approximated by the following function (Chaudhry and Zubair 1994):

$$\Gamma(1/2,u_1;u_2) \cong \frac{1}{2}\sqrt{\pi}\cdot\left[\exp\left(-2\sqrt{u_2}\right)\mathrm{erfc}\left(\sqrt{u_1}-\frac{\sqrt{u_2}}{\sqrt{u_1}}\right) + \exp\left(2\sqrt{u_2}\right)\mathrm{erfc}\left(\sqrt{u_1}+\frac{\sqrt{u_2}}{\sqrt{u_1}}\right)\right] \tag{3.61}$$

For steady-state conditions, applying the method of images to Equation 3.56 yields

$$T(x,y,z) = T_0 + \frac{q_{tb}}{4\pi\lambda_m}\exp\left[\frac{u_t x}{2D_t}\right]\left\{\int_0^H \frac{\exp[-u_t r'/(2D_t)]}{r'} - \int_0^H \frac{\exp[-u_t r'/(2D_t)]}{r'}\right\}\mathrm{d}z_0 \tag{3.62}$$

Introducing the dimensionless variables $R = r/H(L = H)$, $Z = z/H$, $Z' = z_0/H$, $U_1 = R'^2/(4\mathrm{Fo})$, $U_2 = \mathrm{Pe}^2R'^2/16$, and $R'^2 = R^2 + (Z - Z')^2$, we can express Equations 3.60 and 3.62 in dimensionless forms as follows:

$$\Theta_{MFLS} = \exp\left[\frac{\mathrm{Pe}}{2}R\cos\varphi\right]\left\{\int_0^1 \frac{\Gamma(1/2,U_1;U_2)}{\sqrt{\pi}R'}\mathrm{d}Z' - \int_{-1}^0 \frac{\Gamma(1/2,U_1;U_2)}{\sqrt{\pi}R'}\mathrm{d}Z'\right\} \tag{3.63}$$

and for steady-state conditions:

$$\Theta_{MFLS\_steady\text{-}state} = \exp\left[\frac{\mathrm{Pe}}{2}R\cos\varphi\right]\left\{\int_0^1 \frac{\exp[-\mathrm{Pe}\,R'/2]}{R'}\mathrm{d}Z' - \int_{-1}^0 \frac{\exp[-\mathrm{Pe}\,R'/2]}{R'}\mathrm{d}Z'\right\} \tag{3.64}$$

The mean temperature at the borehole wall for the **MFLS** for transient and steady-state conditions is as follows:

$$T(r_0,z) = T_0 + \frac{q_{tb}}{4\pi\lambda_m} I_0\left[\frac{u_t r}{2D_t}\right]\left\{\int_0^H \frac{\exp[-u_t r'/(2D_t)]}{r'} - \int_0^H \frac{\exp[-u_t r'/(2D_t)]}{r'}\right\} dz_0 \tag{3.65}$$

$$T(r_0,z) = T_0 + \frac{q_{tb}}{4\pi\lambda_m} I_0\left[\frac{u_t r}{2D_t}\right]\left\{\int_0^H \frac{\exp[-u_t r'/(2D_t)]}{r'} - \int_{-H}^0 \frac{\exp[-u_t r'/(2D_t)]}{r'}\right\} dz_0 \tag{3.66}$$

$$\Theta_{MFLS} = I_0\left[\frac{Pe}{2}R\right]\left\{\int_0^1 \frac{\Gamma(1/2,U_1;U_2)}{\sqrt{\pi}R'} dZ_0 - \int_{-1}^0 \frac{\Gamma(1/2,U_1;U_2)}{\sqrt{\pi}R'} dZ_0\right\} \tag{3.67}$$

$$\Theta_{MFLS\_steady\text{-}state} = I_0\left[\frac{Pe}{2}R\right]\left\{\int_0^1 \frac{\exp[-Pe\,R'/2]}{R'} dZ_0 - \int_{-1}^0 \frac{\exp[-Pe\,R'/2]}{R'} dZ_0\right\} \tag{3.68}$$

where $R' = \sqrt{R^2 + R_0^2 - 2RR_0\cos\varphi_r' + (Z - Z')^2}$ and $R_0 = r_0/L$.

Figure 3.17 shows the difference between the MFLS and ILS models due to simulation time and borehole length. The longer the simulation time and the shorter the borehole length become, the larger the discrepancy is.

Molina-Giraldo et al. (2011b) concluded that the role of axial effects depends on the groundwater velocity and the length of the BHE. They stated that the MFLS can be applied to all groundwater flow conditions and borehole lengths. However, they also found that the FLS is still valid for Pe < 1.2 and the MILS for Pe > 10.

The **coded functions** (MATLAB scripts) of the **MFLS** model for transient (Equations 3.60 and 3.61) and steady-state (Equation 3.62) conditions are listed as *T_MFLS.m* and *T_MFLSs.m*, respectively. For computing the mean temperature at the borehole wall (Equations 3.65 and 3.66), the coded functions are *T_MFLSc.m* and *T_MFLScs.m*, respectively.

Figure 3.18 compares the relative temperature, ΔT, contours obtained by the MFLS and MILS models with groundwater advection (Molina-Giraldo

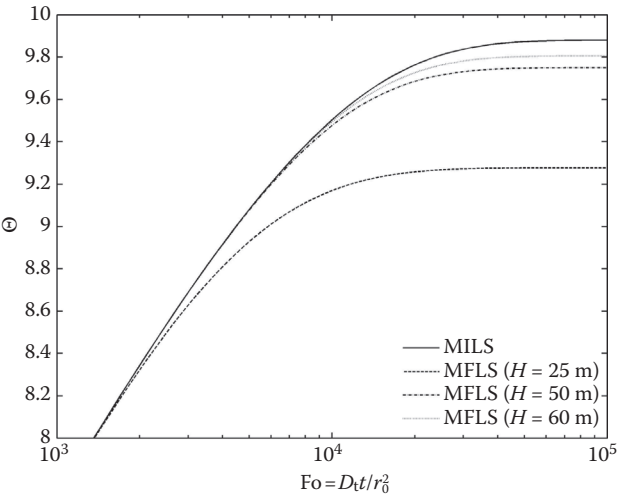

Figure 3.17 Temperature response over dimensionless number Fo for different borehole lengths (q = 1 × 10^{-7} m s^{-1}, D_t = 9 × 10^{-7} m^2 s^{-1}, $x = r_0$ = 0.05 m, y = 0 m, z = 0.5 × H). (Modified after Molina-Giraldo, N. et al. *International Journal of Thermal Sciences* 50 (12), 2506–2513, 2011.)

et al. 2011b). Temperature plumes simulated by the MFLS model are shorter (Figure 3.18a). The reason for this is an axial effect. It induces vertical dissipation of heat and thus leads to lower temperature changes at any lateral distance from the BHE than the MILS. Consequently, by ignoring axial effects, longer boreholes are calculated for the same energy demand by the MILS compared to the MFLS (Marcotte et al. 2010). Figure 3.18b shows the axial extension of the temperature plume. It is revealed that the discrepancies between the MFLS and MILS models are most pronounced close to the endpoints of the borehole.

3.1.9 Infinite plane source—one-dimensional conduction

The **instantaneous plane source** of strength dE/dA (J m^{-2}), within an infinite porous medium is described by a one-dimensional heat conduction equation with constant coefficients, where x is the direction normal to the plane source, and A is the source area:

$$\frac{\partial T}{\partial t} = D_t \frac{\partial^2 T}{\partial x^2} \tag{3.69}$$

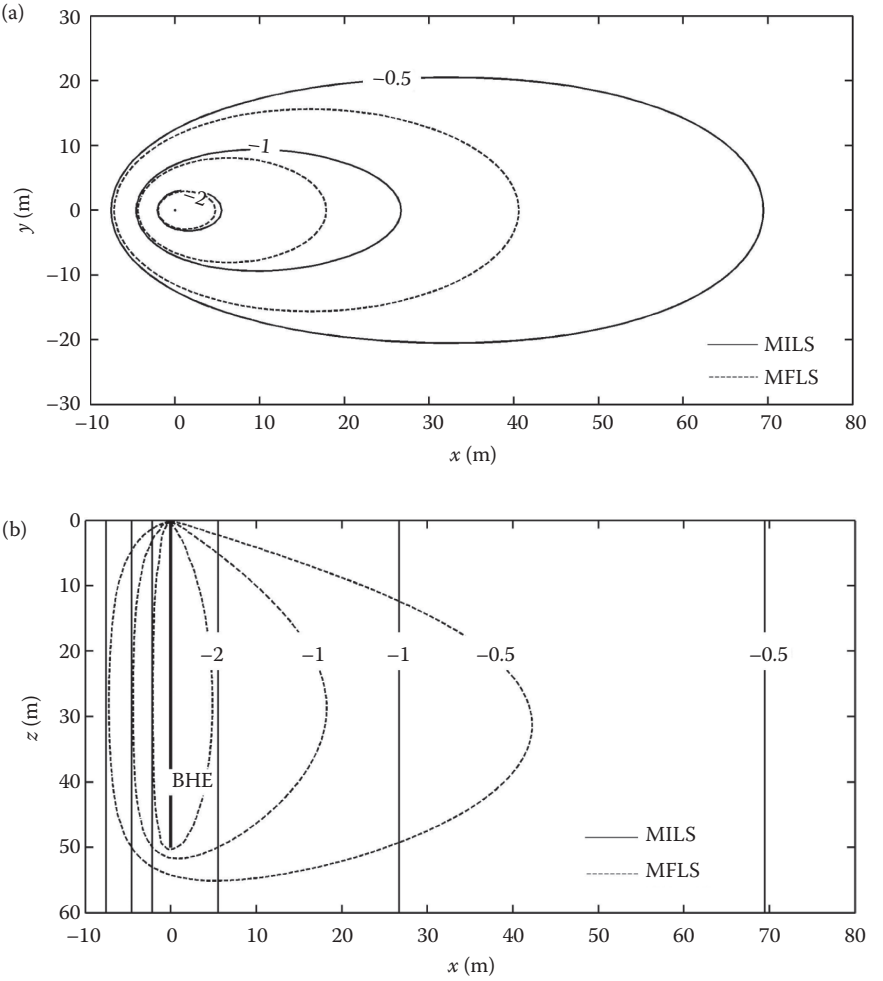

Figure 3.18 Temperature response (K) for a single BHE with constant energy extraction (q_{tb} = J/H = 20 W m^{-1}, q = 1.0 × 10^{-7} m/s, H = 10 m). (a) Plan view (z = 0.5 × H for MFLS). (b) Vertical cross section along centerline (y = 0 m). (Modified after Molina-Giraldo, N. et al. *International Journal of Thermal Sciences* 50 (12), 2506–2513, 2011.)

The initial condition is $T(x,\ t\ =\ 0)\ =\ T_0$. The temperature $T(x,t)$ for a source at the location x_0 is

$$T(x,t) = T_0 + \frac{\Delta E/A}{2 \cdot C_m \cdot (\pi D_t t)^{1/2}} \exp\left(-\frac{(x-x_0)^2}{4D_t t}\right) \tag{3.70}$$

3.1.10 Moving infinite plane source—one-dimensional conduction and advection

The **continuous plane source** of specific strength j (W m^{-2}) within an infinite porous medium consists of a one-dimensional heat conduction and advection problem with the differential equation

$$\frac{\partial T}{\partial t} = D_{\mathrm{t}} \frac{\partial^2 T}{\partial x^2} - u_{\mathrm{t},x} \frac{\partial T}{\partial x} \tag{3.71}$$

The initial condition is $T(x,\ t = 0) = T_0$. The temperature $T(x,\ t)$ for a source at the location x_0 is—after Bear (1979)—in analogy to solute transport:

$$T(x,t) = T_0 + \frac{\Delta T u_{\mathrm{t}}}{(4\pi D_{\mathrm{t,L}})^{1/2}} \exp\left(\frac{u_{\mathrm{t}} \cdot (x - x_0)}{2D_{\mathrm{t,L}}} \right) \int_0^t \frac{1}{\sqrt{\tau}} \exp\left(-\frac{a}{\tau} - b\tau \right) \mathrm{d}\tau \tag{3.72}$$

where a and b are

$$a = \frac{(x - x_0)^2}{4D_{\mathrm{t,L}}}; \quad b = \frac{u_{\mathrm{t}}^2}{4D_{\mathrm{t,L}}} \tag{3.73}$$

and using the steady-state temperature change ΔT:

$$\Delta T = \frac{j}{C_{\mathrm{w}} q} \tag{3.74}$$

The integral may be evaluated numerically. Alternatively, the solution for the **continuous plane source** can be transformed as follows:

$$T(x,t) = T_0 + \frac{\Delta T}{2} \exp\left(\frac{u_{\mathrm{t}} \cdot (x - x_0)}{2D_{\mathrm{t,L}}} \right) \times \left[\exp\left(\frac{-u_{\mathrm{t}} \cdot |x - x_0|}{2D_{\mathrm{t,L}}} \right) \mathrm{erfc}\left(\frac{|x - x_0| - u_t t}{\sqrt{4D_{\mathrm{t,L}} t}} \right) - \exp\left(\frac{u_{\mathrm{t}} \cdot |x - x_0|}{2D_{\mathrm{t,L}}} \right) \mathrm{erfc}\left(\frac{|x - x_0| + u_{\mathrm{t}} t}{\sqrt{4D_{\mathrm{t,L}} t}} \right) \right] \tag{3.75}$$

Note that the products exp(arg1) × erfc(arg2) may have to be evaluated for very large arguments arg1 by combining the series expansion of the two

related functions. The continuous plane source may correspond to a dense array of heat exchangers in the vertical plane of an aquifer with uniform flow conditions.

Dimensionless temperature profiles can be obtained by using the **scaled variables** x', T' and t':

$$x' = \frac{u_t \cdot (x - x_0)}{D_{t,L}}; \quad t' = \frac{u_t^2 t}{D_{t,L}}; \quad T' = \frac{T - T_0}{\Delta T} \tag{3.76}$$

An evaluation is shown in Figure 3.19. Note that **close to the source** at $x' = 0$, thermal **dispersion is overestimated** compared to field observations. This is due to the fact that the combined effect of grain scale mechanical dispersion and macrodispersion depends on the flow distance (Section 2.1.2.3). Both mechanical and macrodispersion start from zero at the source. Therefore, they need some time and flow distance, respectively, until a constant dispersion coefficient is attained. Furthermore, for small times ($t' < 1$), the temperature distribution is almost symmetrical due to the dominance of diffusion and dispersion. For **large times after start of injection** ($t' > 100$), the heat propagation is strongly influenced by advection and can be approximated by

$$T(x,t) \cong T_0 + \frac{\Delta T}{2} \operatorname{erfc}\left(\frac{x' - t'}{2\sqrt{t'}}\right) = T_0 + \frac{\Delta T}{2} \operatorname{erfc}\left(\frac{x - u_t t}{2\sqrt{D_{t,L} t}}\right) \tag{3.77}$$

This solution corresponds to the development of an initially sharp temperature front in an infinite porous medium with $T(x < 0, t = 0)$ and $T(x > 0, t = 0) = T_0 + \Delta T$.

MATLAB scripts of the **infinite plane source** model for transient conductive/dispersive–advective transport (Equation 3.75) and of the **development**

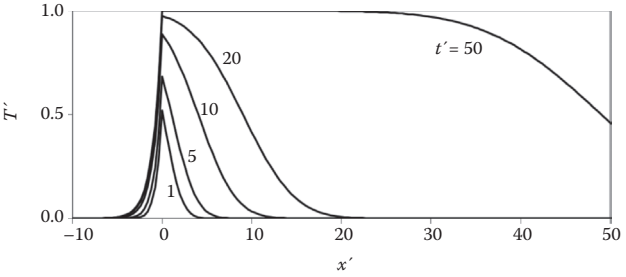

Figure 3.19 Continuous plane source in one-dimensional aquifer. Dimensionless results with $x' = x u_t / D_{t,L}$; $t' = t u_t^2 / D_{t,L}$; $T' = T / T_0$.

of an initially sharp temperature front (Equation 3.77) in a uniform flow field are listed as *Continuous_injection.m* and *Thermal_front.m*, respectively.

3.1.11 Steady-state injection into an aquifer with thermally leaky top layer

The **steady-state, one-dimensional heat transport with thermally leaky top layer** (overburden or cap rock) in a shallow aquifer is described according to Equation 2.113:

$$D_{t,L}\frac{\partial^2 T}{\partial x^2} - u_{t,x}\frac{\partial T}{\partial x} + \frac{j_{vert,top}}{mC_m} = 0 \tag{3.78}$$

where the **thermal flux from the surface to the groundwater** $j_{vert,top}$, considering only heat conduction and assuming constant surface temperature $T_{surface}$, is

$$j_{vert,top} = \frac{\lambda_{vert}\cdot(T_{surface} - T)}{(f + m/2)} \tag{3.79}$$

The **temperature profile** $T(x)$ is the vertically averaged value within the thin aquifer. The temperature before the thermal injection is T_0. The bottom layer is assumed to behave like an insulator. The boundary condition is $T(x\rightarrow\infty) = 0$. The solution for $x \geq 0$ (after Bear 1979) is in analogy to solute transport:

$$T(x) = T_{surface} + \frac{\Delta T}{\chi}\exp\left(\frac{u_t\cdot(x - x_0)}{2D_{t,L}}\cdot(1-\chi)\right) \tag{3.80}$$

with

$$\chi = \left(1 + \frac{4D_{t,L}\lambda_{vert}}{C_m m\cdot(f + m/2)u_t^2}\right)^{1/2} \tag{3.81}$$

If the expression

$$\frac{4D_{t,L}\lambda_{vert}}{C_m m\cdot(f + m/2)u_t^2} \tag{3.82}$$

within Equation 3.81 is small, which is often the case, then $1/\chi \cong 1$, and, using the first term of a series expansion for χ, $(1 - \chi)$ is

$$1-\chi \simeq \frac{2D_{\mathrm{t,L}}\lambda_{\mathrm{vert}}}{C_{\mathrm{m}}m\cdot(f+m/2)u_{\mathrm{t}}^2} \tag{3.83}$$

Thus, the **temperature profile is approximately**

$$T(x) \simeq T_{\mathrm{surface}} + \Delta T \exp\left(\frac{(x-x_0)\lambda_{\mathrm{vert}}}{C_{\mathrm{m}}m\cdot(f+m/2)u_{\mathrm{t}}}\right) = T_{\mathrm{surface}} + \Delta T \exp\left(\frac{(x-x_0)\lambda_{\mathrm{vert}}}{C_{\mathrm{w}}m\cdot(f+m/2)q}\right) \tag{3.84}$$

In this case, the steady-state temperature profile is independent of the coefficient $D_{\mathrm{t,L}}$. Therefore, it cannot be used to estimate $D_{\mathrm{t,L}}$ based on data along a flow line. Instead the profile is determined by the heat flow in the overburden between surface and aquifer. It can be employed to assess the mitigation effect of the overburden for thermal use.

As an **example**, consider the parameter values $D_{\mathrm{t,L}} = 3\ \mathrm{m^2\ day^{-1}}$, $m = 10$ m, $f = 5$ m, $q = 1\ \mathrm{m\ day^{-1}}$, $\lambda_{\mathrm{vert}} = 0.0015\ \mathrm{kJ\ m^{-1}\ K^{-1}\ s^{-1}}$, $C_{\mathrm{w}} = 4200\ \mathrm{kJ\ m^{-3}\ K^{-1}}$, $C_{\mathrm{m}} = 3000\ \mathrm{kJ\ m^{-3}\ K^{-1}}$, and $x_0 = 0$ m. Expression 3.82 is about 0.003, and the approximation 3.84 is well applicable. The temperature at $x = 100$ m is about $T_0 + \Delta T \times 0.97$. For $(T - T_0)/\Delta T = 0.5$, which corresponds to an increase or decrease in the temperature by $\Delta T \times 0.5$ (half-value distance), the flow distance needed is about $x \cong 2200$ m.

3.1.12 Harmonic temperature boundary condition for one-dimensional conductive–advective heat transport

3.1.12.1 One-dimensional vertical conductive heat transport

One-dimensional vertical thermally diffusive transport caused by a **harmonic fluctuation of the surface temperature**, superimposed by a geothermal gradient, is given by the extended classical equation of the periodic temperature profile below the soil surface (Gröber et al. 1955) assuming constant coefficients:

$$T(z,t) = T_{\mathrm{surface}} - Gz + \Delta T \exp\left(z\sqrt{\frac{\pi}{D_{\mathrm{t}}t_{\mathrm{p}}}}\right)\cos\left(z\sqrt{\frac{\pi}{D_{\mathrm{t}}t_{\mathrm{p}}}} + 2\pi\frac{t}{t_{\mathrm{p}}}\right) \tag{3.85}$$

Note that at soil surface, $z = 0$, and with increasing soil depth, $z < 0$. The symbol $T_{surface}$ (K) is the mean soil surface temperature, ΔT (K) is the amplitude of the temperature fluctuation at the surface, G (K m^{-1}) is the geothermal gradient, D_t (m^2 s^{-1}) is the thermal diffusion coefficient of the soil, and t_p (s) is the period of the harmonic temperature development (t_p = 365.25 days for seasonal fluctuations).

3.1.12.2 One-dimensional horizontal conductive/dispersive–advective transport

Let us consider a **horizontal aquifer layer** with uniform flow in the x-direction. Top and bottom layers are assumed to act as **insulators**. One-dimensional horizontal diffusive/dispersive and advective **heat transport** is described by the differential equation

$$\frac{\partial T}{\partial t} = D_{t,L}\frac{\partial^2 T}{\partial x^2} - u_{t,x}\frac{\partial T}{\partial x} \tag{3.86}$$

At location $x = 0$, the **prescribed harmonic temperature boundary condition** applies, for example, as the result from river water inflow with seasonal temperature fluctuation:

$$T(x = 0, t) = T_0 + \Delta T\cos(\omega t) \tag{3.87}$$

The second boundary condition is $T(x \to \infty) = 0$. The coefficient ω is the angular frequency with

$$\omega = \frac{2\pi}{t_p} \tag{3.88}$$

where t_p is the period. The **solution** is of the form (after Burger et al. 1984)

$$T(x, t) = T_0 + \Delta T\exp(-ax)\cos(-bx + \omega t) \tag{3.89}$$

The **coefficients** a and b are the attenuation coefficient and the wave number, respectively. In order to fulfill the differential equation and its boundary conditions, the coefficients are chosen as follows:

$$b = \sqrt{\frac{-\frac{u_t^2}{4D_{t,L}} + \sqrt{\left(\frac{u_t^2}{4D_{t,L}}\right)^2 + \omega^2}}{2D_{t,L}}}; \quad a = \frac{\omega - bu_t}{2bD_{t,L}} \tag{3.90}$$

One-dimensional harmonic horizontal conductive/dispersive–advective transport may correspond to infiltration of river water into an aquifer or to a dense array of heat exchangers with harmonic temperature variation in the vertical plane of an aquifer with uniform flow conditions.

A **scaled evaluation** for the period $t_p = D_{t,L}/u_t^2$ is shown in Figure 3.20. It visualizes the damping effect of thermal conduction and macrodispersion for the selected angular frequency.

If, based on experimental data, the coefficients a and b can be evaluated, the **parameters** u_t and $D_{t,L}$ can be determined as follows:

$$D_{t,L} = \frac{a\omega}{b\cdot(a^2+b^2)}; \quad u_t = \frac{\omega\cdot(a^2-b^2)}{b\cdot(a^2+b^2)} \tag{3.91}$$

As an **illustration**, we select the measured temperature data of Trüeb (1976). He measured temperature time series within a borehole located at a distance of 500 m from the infiltrating River Rhine north of Zurich. Measurements were performed before and after the construction of the dam Rheinau (Figure 3.21), which completely changed the groundwater flow regime after 1957, but not so much the flow direction. From the time delay $\Delta t \cong 180$ day, the coefficient b can be evaluated for the situation before existence of the dam, yielding the angular frequency $\omega = 6.28$ year^{-1} = 0.0172 day^{-1} to be $b \cong 6.2 \times 10^{-3}$ m^{-1}. The temperature amplitude of the river water was $\Delta T_0 \cong 8.3$ K, and in the borehole, an amplitude of $\Delta T_1 \cong 1.5$ K was

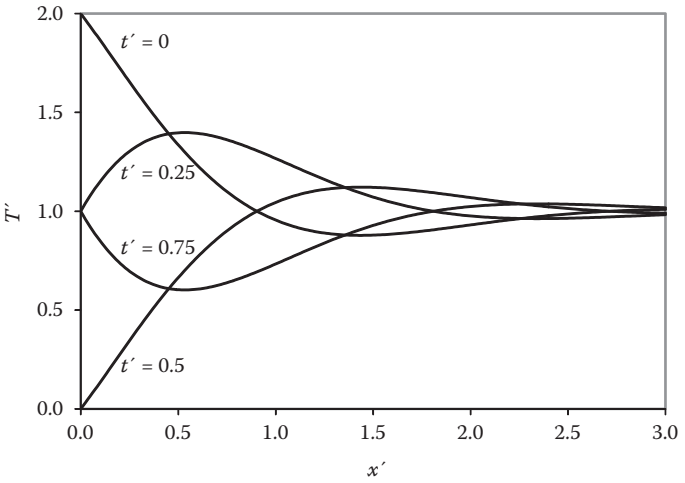

Figure 3.20 Harmonic boundary condition in one-dimensional semi-infinite aquifer. Dimensionless results with $x' = x u_t/D_{t,L}$; $t' = t u_t^2/D_{t,L}$; $T' = T/T_0$. The period is selected according to $u_t^2/D_{t,L} = 1$.

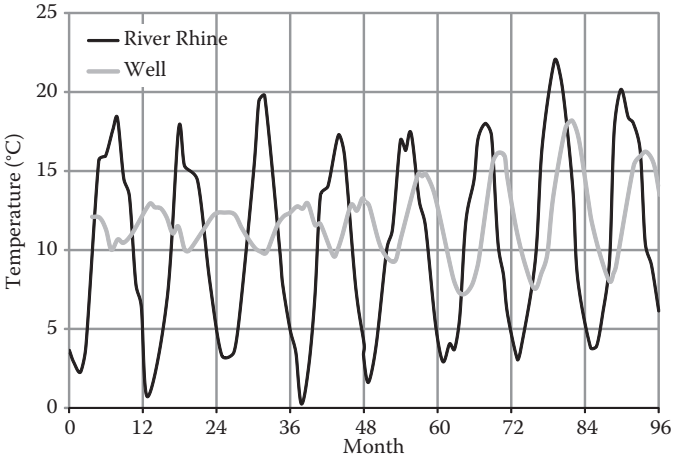

Figure 3.21 Measured temperature of Rhine River and groundwater observation well (500 m from infiltration) before and after the construction of the Rheinau dam (Switzerland) after Trüeb (1976). Month 0 = January 1953: filling from 1957 on (about month 48).

observed. Therefore, the coefficient a is evaluated as $a \cong 3.4 \times 10^{-3}$ m^{-1}, and the coefficients $D_{t,L} \cong 190$ m^2 day^{-1} and $u_t \cong 1.5$ m day^{-1} result from using Equation 3.91. The longitudinal thermal macrodispersivity would be $\beta_L \cong 128$ m. Thermal diffusion can be neglected. For the situation after construction of the dam, the time delay was $\Delta t \cong 84$ day, and the ratio $\Delta T_1/\Delta T_1 \cong 4.5/8.3$. Further, $D_{t,L} \cong 740$ m^2 day^{-1} and $u_t \cong 4.1$ m day^{-1}. The corresponding longitudinal thermal macrodispersivity in that case is $\beta_L \cong 179$ m. The longitudinal thermal dispersivity is roughly constant for both cases. However, we have to keep in mind that the harmonic model assumes that top and bottom layers act as insulators.

Equation 3.89 can also be applied to the vertical case as described in Section 3.1.12.1, including the assumption of constant vertical thermal advection due to uniform recharge.

A MATLAB script of the model for one-dimensional **harmonic thermal conductive/dispersive–advective transport** (Equations 3.89 and 3.90) is listed as *Harmonic_temperature.m*.

3.1.12.3 Horizontal layer embedded in conductive bottom and top layer

An **analytical approximation** can be formulated by taking the effect of thermally conductive bottom and top layers into account. The prerequisite is that both layers are homogeneous and are both sufficiently thick. For example, in order to exclude an influence of the soil surface, the distance

from soil surface to groundwater table has to be large enough. The one-dimensional **transient differential equation** for the horizontal aquifer layer reads as follows:

$$\frac{\partial T}{\partial t} = D_{t,L}\frac{\partial^2 T}{\partial x^2} - u_{t,x}\frac{\partial T}{\partial x} + \frac{j_{vert,top}}{C_m m} + \frac{j_{vert,bottom}}{C_m m} \tag{3.92}$$

with

$$j_{vert,top} = -\lambda_{top}\left(\frac{\partial T}{\partial z}\right)_{y=0}; \quad j_{vert,bottom} = \lambda_{bottom}\left(\frac{\partial T}{\partial z}\right)_{y=0} \tag{3.93}$$

The concept for the horizontal temperature development in the aquifer layer is still the same as in Equation 3.89. For the **vertical temperature fluctuation**, the following approach is taken:

$$T(x, y, t) = T_0 + \Delta T\exp(-ax - a_0 y)\cos(-bx - b_0 y + \omega t) \tag{3.94}$$

with

$$\begin{aligned} &a_0 = b_0; \quad b_0 = \sqrt{\frac{\omega}{2D_0}}; \\ &\lambda_0 = \lambda_{top} = \lambda_{bottom} = D_0 C_0; \\ &D_0 = D_{top} = D_{bottom}; \\ &C_0 = C_{top} = C_{bottom}; \end{aligned} \tag{3.95}$$

The vertical coordinate y_0 starts at the upper and lower aquifer layer boundary. In order to fulfill the differential equation and its boundary conditions, the **coefficients** a and b are chosen as follows:

$$\begin{aligned} &b = \sqrt{\frac{-\left(\frac{u_t^2}{4D_{t,L}} + \eta\right) + \sqrt{\left(\frac{u_t^2}{4D_{t,L}} + \eta\right)^2 + (\omega + \eta)^2}}{2D_{t,L}}}; \\ &a = \frac{\omega + \eta - bu_t}{2bD_{t,L}}; \\ &\eta = \sqrt{2\omega D_0}\,\frac{C_0}{C_m m} \end{aligned} \tag{3.96}$$

Given the coefficients a and b, the **parameters** $D_{t,L}$ and u_t are evaluated as follows:

$$D_{t,L} = \frac{\omega - \sqrt{2\omega D_0}\,\frac{C_0}{C_m m}\cdot\left(\frac{b}{a}-1\right)}{\frac{b}{a}\cdot(a^2+b^2)};$$
$$u_t = \frac{D\cdot(a^2-b^2)+\sqrt{2\omega D_0}\,\frac{C_0}{C_m m}}{a} \qquad (3.97)$$

For $D_0 = 0$, Equation 3.91 is obtained.

The **illustrative example** of Section 3.1.12.2 with the infiltration of river water and the estimation of the parameters before and after the construction of the dam in the Rhine River can thus be reevaluated. Using the same coefficients a and b, the parameters $D_{t,L}$ and u_t are obtained as follows, assuming $C_0 = 1.6 \times 10^6$ J m^{-3} K^{-1}, $C_m = 2.4 \times 10^6$ J m^{-3} K^{-1}, and $D_0 = 0.0972$ m^2 day^{-1}. Before construction of the dam, the parameters were $D_{t,L} \cong 167$ m^2 day^{-1}, $u_t \cong 1.3$ m day^{-1}, and $\beta_L \cong 128$ m. After construction of the dam, they were $D_{t,L} \cong 614$ m^2 day^{-1}, and $u_t \cong 3.4$ m day^{-1}, and $\beta_L \cong 178$ m. The comparison with Section 3.1.12.2 shows that the top and bottom layers may show a distinct influence on the parameters. However, interestingly, the values for longitudinal thermal macrodispersivity did not change with the new model. Again, very roughly, it is about constant for both cases. It has to be mentioned that the sensitivity of the parameters with respect to the values of a and b is relatively large.

3.2 OPEN SYSTEMS

Open systems in shallow aquifers often consist of one or several extraction wells and facilities for the injection into more or less uniform flow fields, which can be modeled as local infiltration wells. An overview on available analytical solutions for open systems is given in Table 3.1. This table shows that heat conduction is treated differently depending on the analytical solution. The analytical approach presented by Guimerà et al. (2007), for instance, does not account for heat transfer into the confining layers. On the other hand, some analytical approaches do not account for heat conduction within the aquifer (Lauwerier 1955; Malofeev 1960; Yang and Yeh 2008). In the following, we present some analytical solutions to flow and heat transport problems.

Table 3.1 Available analytical solutions for open systems

	Flow type			*Heat conduction in aquifer*		*Heat conduction in confining layers*		*Top boundary condition*	
Source	*Linear*	*Radial*	*Arbitrary*	*Linear*	*Radial*	*Caprock*	*Bedrock*	*Variable temperature*	*Heat exchange*
Lauwerier (1955)	x					inf	inf		
Malofeev (1960)		x				inf	inf		
Avdonin (1964)	x			x		inf	inf		
Avdonin (1964)		x			x	inf	inf		
Guimerà et al. (2007)		x			x	–	–		
Chen and Reddell (1983)		x			x	inf	inf		
Voigt and Haefner (1987)		x			x	fin	inf	x	
Güven et al. (1983)		x			x	fin	inf		x
Yang and Yeh (2008)		x				fin	fin		
Gringarten and Sauty (1975)			x			inf	inf		

Note: inf: infinite extent; fin: finite extent (constant aquifer thickness).

3.2.1 Analytical solution for steady-state flow in multiple well systems

Open systems are often operated at quasi–steady state. Therefore, **steady-state flow in multiple well systems of idealized two-dimensional aquifers with uniform flow** is of high interest. In this section, we would like to recall results of analytical solutions for the computation of isolines for **piezometric head** and **stream function** as a result of local sources and sinks (constant rate recharging and/or pumping wells, single wells, or series of wells) in a uniform horizontal flow field of an **infinite and confined aquifer without areal recharge**. The hydraulic conductivity K_w, as well as the thickness m of the aquifer, are assumed to be constant. The computation is performed analytically, and graphs of isolines of both the head and the stream function can be produced. The results are also approximately valid for phreatic aquifers, provided that the rise and decline of the groundwater table are small compared to the thickness of the aquifer.

The computation is performed in a homogeneous horizontal x–y system making use of the **superposition principle**. According to the potential flow theory, the specific discharge vector can be expressed by

$$\mathbf{q} = -K_w \nabla h_w = -\nabla \varphi \tag{3.98}$$

where φ is the velocity potential with $\varphi = K_w h_w$. For a **uniform flow field**, the velocity potential is given by

$$\varphi(x, y) = -q_0 \cdot (x\cos\alpha + y\sin\alpha) \tag{3.99}$$

q_0 is the specific flux of the regional flow field, and α is the flow direction with respect to the x-axis (Figure 3.22). The stream function $\psi(x, y)$ of the uniform flow field is

$$\psi(x, y) = -q_0 \cdot (y\cos\alpha + x\sin\alpha) \tag{3.100}$$

For a **single well** (Figure 3.23), the velocity potential is (Bear 1979)

$$\varphi(x,y) = \frac{Q/m}{4\pi} \ln\left(\frac{(x - x_w)^2 + (y - y_w)^2}{R_w^2} \right) \tag{3.101}$$

where Q is the recharge or pumping rate ($Q > 0$: recharge; $Q < 0$: pumping); x_w and y_w are the coordinates of the well. R_w is the radius of influence of the well, and m is the aquifer thickness. An influence of the finite well

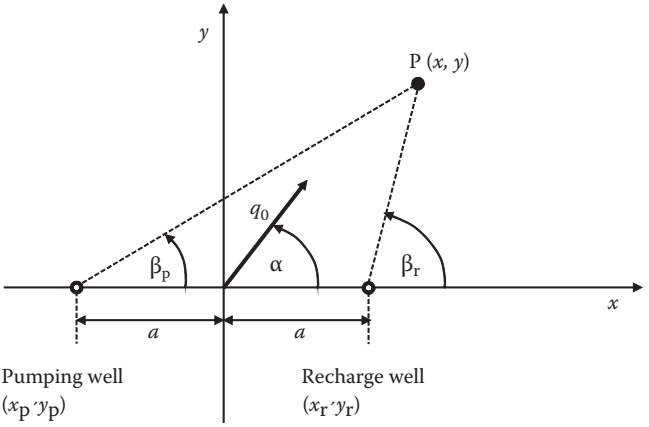

Figure 3.22 Double well system with recharge well and pumping well in uniform flow field q_0.

radius r_w on the flow is disregarded. The stream function of a single well (Figure 3.23) is

$$\psi(x,y) = \frac{Q/m}{2\pi} \tan^{-1}\left(\frac{y-y_w}{x-x_w}\right) \tag{3.102}$$

The computation of the head around a single well is based on the concept of a finite radius of influence of the well. According to this concept, it is

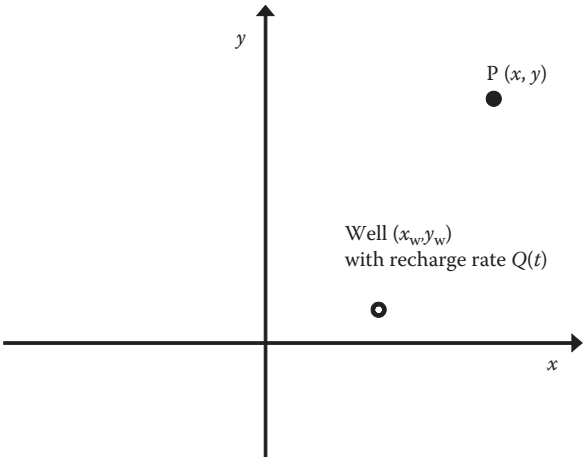

Figure 3.23 Well with recharge rate Q_w and observation point P.

assumed that the decline or rise of the head is zero at a distance of R_w. The result is only approximately valid inside of the zone of influence. Outside of the zone, results are inaccurate. In the case of a **two-well system** (Figure 3.22) with pumping and recharging wells of opposite recharge and pumping rate $\pm Q$ and same well radius r_w, the result of the superposition is valid in the whole domain regardless of the value of R_w (also outside of the zone of influence). The result is then independent of the radius of R_w. The same result is obtained by a consideration of a straight constant head line (e.g., a river or lake) by applying the **method of images** (introduction of a fictitious image well with opposite rate). In general, the solution becomes independent of the radius R_w if the pumping and infiltration rates of all wells sum up to zero.

An example of the flow field for a system with one pumping well and two injection wells with $Q_P = -2Q_R$ in a uniform flow field aligned with the direction defined by the pumping well and the central point between the two recharging wells is shown in Figure 3.24 in scaled form. The length scale is the half-distance a between the pumping well and the center between the recharge wells. Regional flow with specific discharge q_0 is from left to right. The pumping rate is chosen as $Q_P = \pi m\, aq_0$. It can be

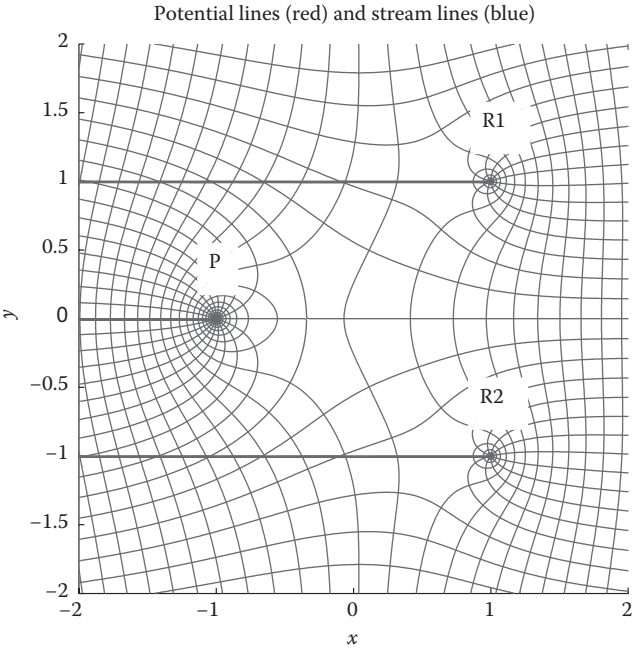

Figure 3.24 **(See color insert.)** Scaled flow field with $\alpha = 0$ and scaled pumping rate; one pumping well and two injection wells. P: pumping well; R1, R2: recharge wells.

seen that downstream of the pumping well, a stagnation point appears. Two further stagnation points are located upstream of the recharge wells. Furthermore, it can be seen that stream tubes from the regional flow pass between the wells. Note that the thick blue line in Figure 3.24 is due to the discontinuity of the stream function caused by the wells. The discontinuity is not necessarily a streamline.

3.2.1.1 Double well system in uniform flow field

The **velocity potential of a double well system with pumping and recharging well in a uniform flow field** with direction α (Figure 3.22), where both the recharge well and the pumping well have the same constant discharge rate Q (>0), is (DaCosta and Bennett 1960)

$$\varphi(x,y) = -q_0 \cdot (x\cos\alpha + y\sin\alpha) + \frac{Q/m}{4\pi}\ln\left(\frac{(x+a)^2+y^2}{(x+a)^2+y^2}\right) \tag{3.103}$$

The symbol a is the half-distance between the wells. The **corresponding stream function** is (DaCosta and Bennett 1960)

$$\begin{aligned}\psi(x,y) &= -q_0 \cdot (y\cos\alpha - x\sin\alpha) + \frac{Q/m}{2\pi}(\theta_r - \theta_p) \\ &= -q_0 \cdot (y\cos\alpha - x\sin\alpha) + \frac{Q/m}{2\pi}\tan^{-1}\left(\frac{2ay}{a^2 - x^2 - y^2}\right)\end{aligned} \tag{3.104}$$

By introducing the **dimensionless pumping rate** χ with

$$\chi = \frac{Q}{\pi m a q_0} \tag{3.105}$$

and dividing Equation 3.104 by the pumping rate, we obtain

$$\frac{\psi(x,y)}{Q/m} = -\frac{1}{\pi\chi}\cdot\left(\frac{y}{a}\cos\alpha - \frac{x}{a}\sin\alpha\right) + \frac{1}{2\pi}(\theta_p - \theta_r) \tag{3.106}$$

For **flow parallel to the *x*-axis** (angle α = 0), the flow field is shown in Figure 3.25 for the dimensionless pumping rates β = 0.5 (weak discharge rate; Figure 3.25a), β = 1 (Figure 3.25b), and β = 2 (strong discharge rate; Figure 3.25c). By analyzing these flow fields, it can be seen that for β = 0.5 (Figure 3.25a), the limiting streamlines of the wells, which define the well

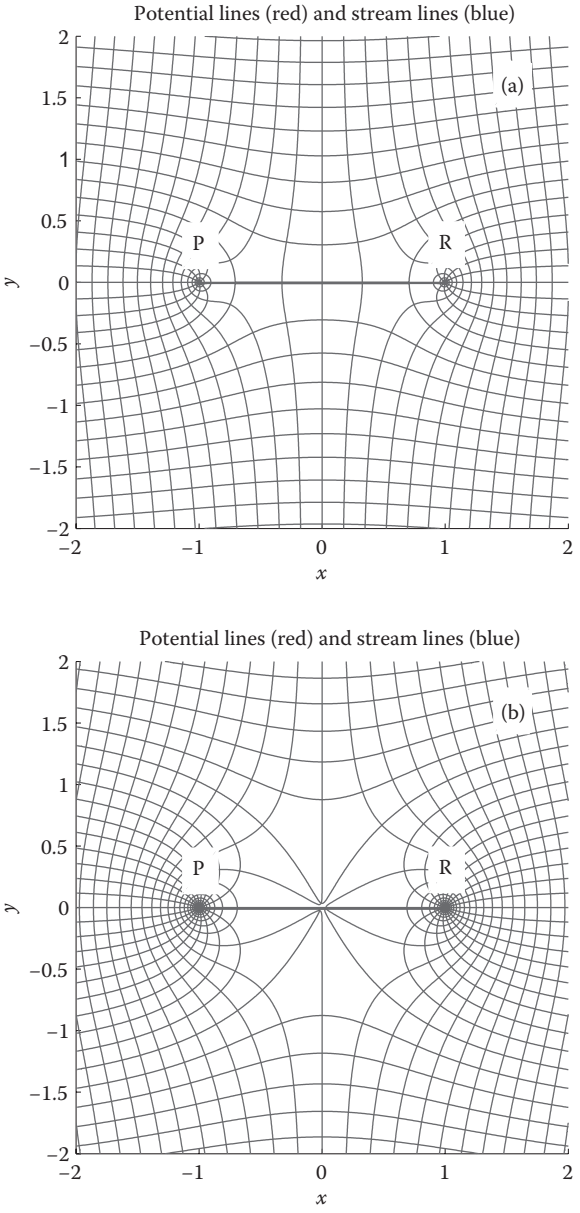

Figure 3.25 **(See color insert.)** (a) Scaled flow field with $\alpha = 0$ and scaled pumping rate $\chi = 0.5$. P: pumping well; R: recharge well. (b) Scaled flow field with $\alpha = 0$ and $\chi = 1$. (c) Scaled flow field with $\alpha = 0$ and $\chi = 2$. (d) Scaled flow field with $\alpha = 90°$ and $\chi = 1$.

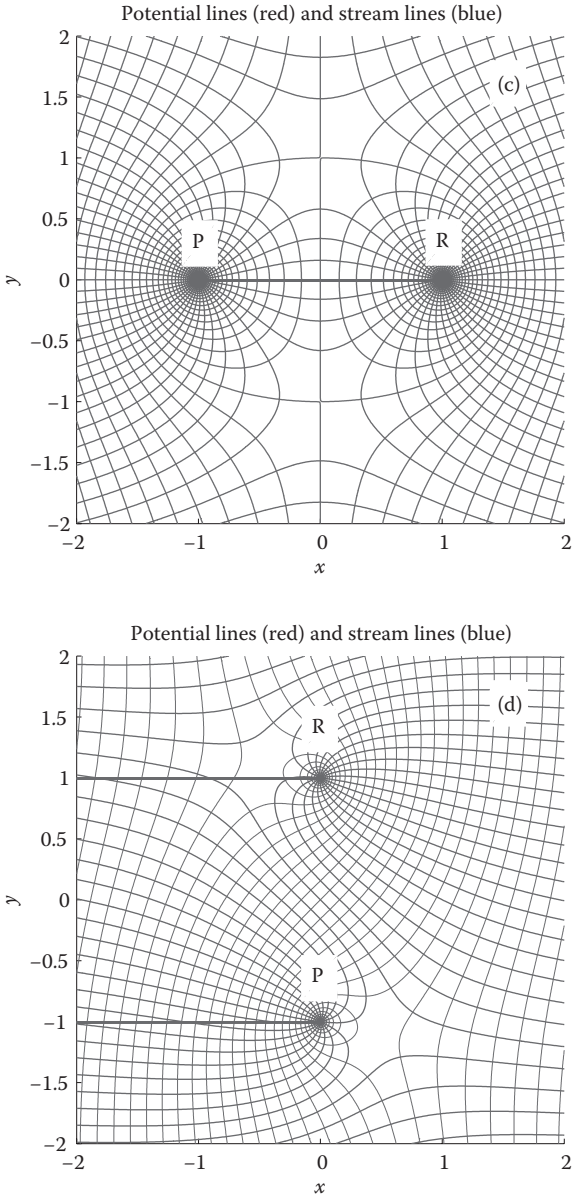

Figure 3.25 (Continued) (a) Scaled flow field with $\alpha = 0$ and scaled pumping rate $\chi = 0.5$. P: pumping well; R: recharge well. (b) Scaled flow field with $\alpha = 0$ and $\chi = 1$. (c) Scaled flow field with $\alpha = 0$ and $\chi = 2$. (d) Scaled flow field with $\alpha = 90°$ and $\chi = 1$.

recharge and discharge regions, are well separated from each other. Part of the region between the wells is flushed by regional flow. This situation is characterized by two stagnation points along the x-axis. For $\beta = 2$ (Figure 3.25c), the limiting streamlines of the wells intersect and show a distinct recirculation between the wells. This effect is visible by the fact that one or more stream tubes start at the recharge well and end at the pumping well. In this case, two stagnation points appear along the y-axis. For the critical case with $\beta = 1$ (Figure 3.25b), the limiting streamlines join at point $x = 0$, $y = 0$, which is the only stagnation point. The three cases can also be characterized by analyzing the location of the stagnation points. In general, two stagnation points show up. At a **stagnation point**, by definition, the components q_x and q_y of the discharge vector vanish, that is (for $\alpha = 0$),

$$\begin{aligned} q_x(x_s, y_s) &= q_0 + \frac{Q}{2\pi m} \cdot \left[-\frac{(a - x_s)}{(a - x_s)^2 + y_s^2} - \frac{(a + x_s)}{(a + x_s)^2 + y_s^2} \right] = 0 \\ q_y(x_s, y_s) &= \frac{Q}{2\pi m} \cdot \left[-\frac{y_s}{(a - x_s)^2 + y_s^2} - \frac{y_s}{(a + x_s)^2 + y_s^2} \right] = 0 \end{aligned} \tag{3.107}$$

These two equations can be rearranged as follows:

$$\begin{aligned} &\frac{Qa}{\pi m q_0} \cdot \left[-\left(a^2 - x_s^2\right) - y_s^2 \right] + \left[\left(a^2 + x_s^2 + y_s^2\right)^2 - 4a^2 x_s^2 \right] = 0 \\ &\frac{Qa}{\pi m q_0} 2 x_s y_s = 0 \end{aligned} \tag{3.108}$$

For this system, two solutions exist, one for $x_s = 0$, and one for $y_s = 0$. For $x_s = 0$ (for $\alpha = 0$)

$$y_s = \pm a \sqrt{\frac{Q}{\pi m a q_0} - 1} = \pm a \sqrt{\chi - 1} \tag{3.109}$$

which is meaningful for $\chi \geq 1$. This situation corresponds to Figure 3.25c. Equation 3.109 defines two stagnation points in general.

For the other case with $y_s = 0$ (for $\alpha = 0$)

$$x_s = \pm a \sqrt{1 - \frac{Q}{\pi m a q_0}} = \pm a \sqrt{1 - \chi} \tag{3.110}$$

which is meaningful for $\chi \leq 1$. This situation corresponds to Figure 3.25a. For the **critical case** with $\chi = 1$ (Figure 3.25b), $x_s = 0$ and $y_s = 0$. In this case, the two stagnation points merge to one at the origin. This is the case with minimum distance between the wells, where no recirculation between the wells occurs. Recirculation between the wells can be analyzed by evaluating the stream function passing through one stagnation point and the two wells and the stream function passing through the origin (DaCosta and Bennet 1960). Taking the difference yields half the recirculation rate. The total recirculation rate I can be expressed by using information on stagnation point S_1:

$$I = 2 \cdot [\psi(x_{s1}, y_{s1}) - \psi(0, 0^+)] = 2 \cdot \left[\psi(x_{s1}, y_{s1}) + \frac{Q}{2m} \right] \tag{3.111}$$

or with information of stagnation point S_2:

$$I = 2 \cdot [\psi(0, 0^-) - \psi(x_{s2}, y_{s2})] = 2 \cdot \left[\frac{Q}{2m} - \psi(x_{s2}, y_{s2}) \right] \tag{3.112}$$

The recirculation rate denotes the rate that stems from the recharge well. Note the singularity of the stream function at the origin. Recirculation is characterized by a positive value. Negative values are an indication for the amount of regional flow between the wells. In such a case, no recirculation occurs. After insertion of the coordinates of one stagnation point, the recirculation rate divided by the discharge rate Q is for $\chi \geq 1$ and $\alpha = 0$ (Bear 1979):

$$\frac{I}{Q} = \frac{2}{\pi} \left[-\frac{1}{\chi} \sqrt{\chi - 1} + \tan^{-1} \left(\sqrt{\chi - 1} \right) \right] \tag{3.113}$$

The **recirculation rate I between the wells is zero** for $\chi = 1$, which has already been referred to as **critical case**. The corresponding half-distance a between the wells is for $\alpha = 0$:

$$a = \frac{Q}{\pi m q_0} \tag{3.114}$$

The related distance between the wells is $d = 2a$. Equation 3.114 represents the **basis for the design of double well systems in parallel flow, aligned with the direction defined by the two wells** ($\alpha = 0$). Therefore, it has been used in the past in open systems for thermal use of shallow aquifers in

order to avoid recirculation and thus avoid pumping of cool or warm water stemming from the injection well. Note that the considerations are based on pure advection, thus neglecting thermal diffusion and transverse dispersion effects.

For the case where the **flow field is not aligned with the direction defined by the two wells**, that is, $\alpha \neq 0$, the **location of the stagnation points** can be found best by applying the theory of complex numbers (DaCosta and Bennett 1960):

$$\frac{x_s}{a} = \mp\sqrt{\frac{1}{2}\left[1-\chi\cos\alpha+\sqrt{1+\chi^2-2\chi\cos\alpha}\right]}$$
$$\frac{y_s}{a} = \pm\sqrt{\frac{1}{2}\left[\chi\cos\alpha-1+\sqrt{1+\chi^2-2\chi\cos\alpha}\right]} \tag{3.115}$$

The permissible pairs of x_s and y_s are those of opposite sign. Recirculation between wells can be evaluated in a similar manner as stated above (Equations 3.111 and 3.112) by using the stream function at the stagnation points and the origin.

Evaluations of the recirculation by DaCosta and Bennet (1960) for **different angles** α indicate that for the critical case with $\chi = 1$, there is **no recirculation** for the angles $-101° \leq \alpha \leq 101°$. They further showed that the angle α_{min} for minimum recirculation is

$$\cos\alpha_{min} = \frac{Q}{2\pi a q_0} = \frac{\chi}{2} \tag{3.116}$$

For $\alpha = 60°$, the amount of regional flow is maximum with $I/Q = -0.14$. This means that the design of the two-well system using Equation 3.114 is quite robust with respect to variations in the angle α of the regional flow field. For the ratio $\chi = 4/\pi = 1.273$, recirculation between the wells occurs except at the angle $\alpha = 50.46°$. This means that, theoretically, solutions without recirculation exist, where the half-distance a between the wells can be chosen to be smaller than the value in Equation 3.114. The corresponding value for the half-distance a would be

$$a_{min} = \frac{Q}{4mq_0} \tag{3.117}$$

as stated, for example, by Mehlhorn et al. (1981). However, if recirculation has to be prevented, this situation is not recommended due to the variability and uncertainty of the angle α of the flow field in practice.

An example with $\alpha = 90°$ and $\chi = 1$ is shown in Figure 3.25d. As can be seen, stream tubes from regional flow pass between the wells. Therefore, it is obvious that no recirculation occurs, as already expected from the discussion above. The related regional flow compared with Q is about –0.06 (no recirculation).

A **program** (MATLAB script) to visualize steady-state flow nets (head and stream function isolines) for multiple well systems in a uniform flow field is *wells_in_flow_field.m*. Note that the stream function for wells shows a distinct singularity (step). It is plotted as a thick blue line. Streamlines across this singularity line are not necessarily continuous. Often, continuity of streamlines can be achieved by proper choice of minimum and step values of the stream function contours.

The **coded function** (MATLAB script) for calculating the recirculation rate and the fraction of recirculation at the total pumping rate Q of double well systems is listed as *recirculation_rate.m*. For example, wells of a half-distance $a = 100$ m, which are aligned with the flow field at the angle $\alpha = 0$, with the pumping rate $Q = 4000$ m^3 day^{-1} in an aquifer of thickness $m = 10$ m, and a Darcy velocity $q_0 = 1$ m day^{-1}, yield a recirculation rate of $I = 18.1$ m^3 day^{-1} and a fraction of 0.0045 of water from the recharge well.

Lippmann and Tsang (1980) addressed the **problem of advective thermal breakthrough time at the pumping well** of a double well system, where the **flow is aligned with the direction between infiltration and pumping well** ($\alpha = 0$, Figure 3.22). The breakthrough time is the time that is needed for the thermal front after starting a double well system to reach the pumping well. Thermal diffusion and dispersion are disregarded.

For the situation where **no regional flow** exists (i.e., $q_0 = 0$), the **breakthrough time** t_b is (Lippmann and Tsang 1980)

$$t_b = \frac{\pi\phi m d^2}{3Q} \cdot \frac{C_m}{\phi C_w} = \frac{\pi\phi m d^2}{3Q} \cdot R_{t\_ret} \tag{3.118}$$

where R_{t_ret} is the thermal retardation factor after Equation 2.98, $d = 2a$ is the distance between the wells, and Q is the pumping and infiltration rate. Lippmann and Tsang (1980) also provide an analytic approximation for the temperature development $T(t)$ at the pumping well.

For the case where between pumping well and injection well a **flow field** $q_0 > 0$ exists, the **breakthrough time** is determined by (Lippmann and Tsang 1980)

$$t_b = \frac{dR_t\phi}{q_0} \cdot \left[1 - \frac{4A}{\sqrt{4A-1}} \tan^{-1}\left(\frac{1}{\sqrt{4A-1}}\right)\right] \tag{3.119}$$

where the auxiliary variable A is

$$A = \frac{Q}{2\pi m d q_0} \tag{3.120}$$

provided that the specific flow rate of the flow field q_0 is smaller than that of the critical case according to Equation 3.114, that is,

$$q_0 < \frac{2Q}{\pi m d} \tag{3.121}$$

For larger flow rates, the breakthrough time is infinite or does not exist. The latter is also applicable for $q_0 < 0$, that is, a flow direction from injection well to pumping well.

3.2.2 Linear flow

Pioneering work by Lauwerier (1955) presented an analytical solution in which the flow pattern is linear. Heat conduction is considered in the vertical direction toward the confining layers, which are assumed infinite in the z-direction (Figure 3.26). The analytical solution is as follows:

$$\bar{T}(\tau, \xi, \eta) = \operatorname{erfc}\left[\frac{\xi + |\eta| - 1}{2\sqrt{\theta(\tau - \xi)}}\right] U(\tau - \xi) \tag{3.122}$$

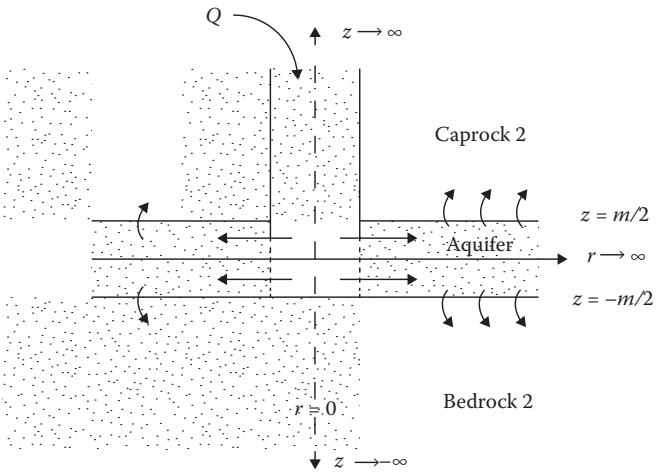

Figure 3.26 Conceptual model of Lauwerier (1955) analytical solution. (Modified after Voigt, H.D. and Haefner, F., *Water Resources Research* 23 (12), 2286–2292, 1987.)

subject to the following condition:

$$U(\tau-\xi)=0 \quad \text{if } \tau-\xi\le 0$$
$$U(\tau-\xi)=1 \quad \text{if } \tau-\xi>0 \tag{3.123}$$

The quantities $\bar{T}$, ξ, η, τ, and θ are dimensionless variables defined as

$$\bar{T}=\frac{T-T_0}{T_{\text{inj}}-T_0},\ \theta=\frac{C_{\text{m}}}{C_{\text{m2}}},\ \tau=\frac{4\lambda_{\text{m2}}t}{m^2C_{\text{m}}},\ \xi=\frac{4\lambda_{\text{m2}}x}{m^2C_{\text{w}}q_0} \tag{3.124}$$

$$\eta=\frac{2z}{H}\ \text{for}\ z\ge\frac{m}{2} \tag{3.125}$$

where T_0 denotes the initial temperature of the aquifer, T_{inj} is the injection temperature, and C_{m2} and λ_{m2} are the volumetric heat capacity and thermal conductivity of the confining layers, respectively.

Avdonin (1964) gets rid of one of the restrictions from Lauwerier (1955) by adding thermal conduction also in the flow direction (*x*-direction). The analytical solution is as follows:

$$\bar{T}=\frac{\bar{x}}{\sqrt{\pi\lambda_{\text{e}}\tau}}\int_0^1\exp\left[-\left(\gamma\sqrt{\lambda_{\text{e}}\tau}\psi-\frac{\bar{x}}{2\sqrt{\lambda_{\text{e}}\tau}\psi}\right)^2\right]\text{erfc}\left(\frac{\sqrt{\tau/\lambda_{\text{e}}}\psi^2}{2a\sqrt{1-\psi^2}}\right)\frac{\text{d}\psi}{\psi^2} \tag{3.126}$$

where:

$$\lambda_{\text{e}}=\lambda_{\text{m}}/\lambda_{\text{m2}};\ \gamma=\frac{mq_0C_{\text{w}}}{4\lambda_{\text{m}}};\ \bar{x}=\frac{2x}{m};\ a=\sqrt{\frac{\lambda_{\text{m2}}C_{\text{m}}}{\lambda_{\text{m}}C_{\text{m2}}}} \tag{3.127}$$

Further details of the equations from Lauwerier (1955) and Avdonin (1964) can be found in Spillette (1965). Figure 3.27 shows the comparison of the two equations considering linear flow. The only difference lies in the consideration of thermal conduction in the longitudinal direction of Equation 3.126.

The **coded functions** (MATLAB scripts) of Equations 3.122 and 3.126 are listed as *T_lau_linear.m* and *T_avd_linear.m*, respectively. As an example, Figure 3.28 shows the temperature response at 1 m downstream from the injection well. Consideration of thermal conduction in the longitudinal direction (Equation 3.126) results in a smooth temperature response.

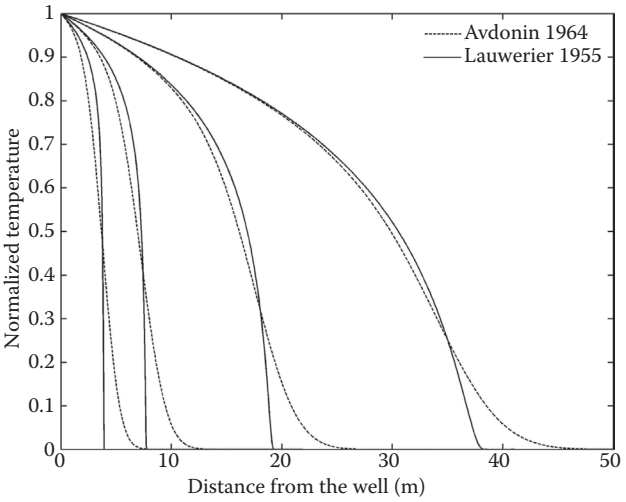

Figure 3.27 Normalized temperature $\bar{T} = (T - T_0)/(T_{inj} - T_0)$ as a function of distance for linear flow equations ($q_0 = 1 \times 10^{-5}$ m s^{-1}, $m = 10$ m, $\lambda_m = \lambda_{m2} = 2.5$ W m^{-1} K^{-1}). Temperature profiles shown at 10, 20, 50, and 100 days.

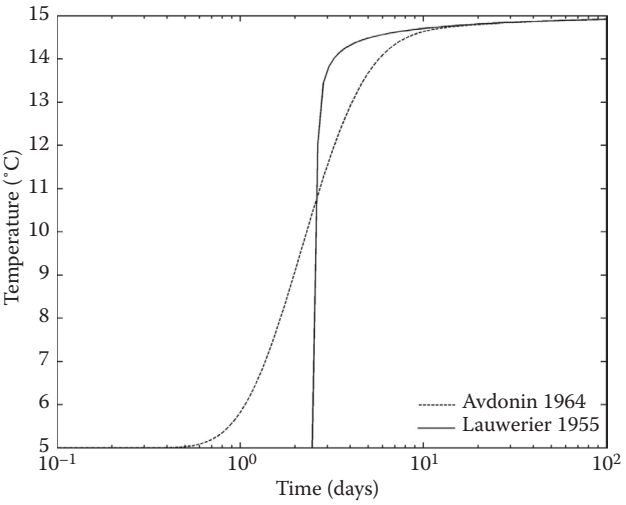

Figure 3.28 Temperature response over time at 1 m downstream from injection well ($q_0 = 1 \times 10^{-5}$ m s^{-1}, m = 10 m, $m\lambda_m = \lambda_{m2} = 2.5$ W m^{-1} K^{-1}). Equation 3.122: Lauwerier (1955); Equation 3.126: Avdonin (1964).

3.2.3 Radial flow, infinite disk source

Guimerà et al. (2007) modify the two-dimensional transient solute transport analytical solution after Gelhar and Collins (1971), which estimates contaminant distribution in porous media due to a fully penetrating injection well for zero flow conditions, used for calculating the temperature distribution due to an injection well of a groundwater heat pump system. The modified equation for horizontal conductive heat transport, from a continuous point source without groundwater flow after Guimerà et al. (2007), is given by

$$\bar{T} = \frac{T - T_0}{T_{\text{inj}} - T_0} = \frac{1}{2}\operatorname{erfc}\left[\frac{r^2 - R_{\text{tw}}^2}{2\left[\frac{4\beta_{\text{L}} R_{\text{tw}}^3}{3} + \frac{\lambda_{\text{m}} R_{\text{tw}}^4}{C_{\text{m}} A_{\text{T}}}\right]^{1/2}}\right] \tag{3.128}$$

where R_{tw} represents the thermal radius of influence.

$$R_{\text{tw}} = \sqrt{2 A_{\text{T}} t} \tag{3.129}$$

$$A_{\text{T}} = \frac{Q C_{\text{w}}}{2\pi m C_{\text{m}}} \tag{3.130}$$

The previous analytical solution does not take axial effects into account. It assumes that there is no heat exchange with the upper and lower layers. For radial type flow, however, when there is a minor influence of the natural groundwater flow, axial effects might become important, especially for long-term simulations. Malofeev (1960) and Avdonin (1964) present analytical solutions with radial flow considering axial effects. Malofeev (1960) slightly modified the Lauwerier solution in order to apply it to radial flow. The dimensionless parameters shown in Equation 3.125 are changed as follows:

$$\xi = \frac{4\lambda_{\text{m2}} \pi r^2}{m C_{\text{w}} Q} \tag{3.131}$$

As in the linear flow, Avdonin (1964) adds thermal conduction in the horizontal direction, resulting in the following equation:

$$\bar{T} = \frac{1}{\Gamma(\nu)}\left[\frac{\overline{r^2}}{4\lambda_{\text{e}}\tau}\right]^{\nu} \int_0^1 \exp\left[-\frac{\overline{r^2}}{4\lambda_{\text{e}}\tau y}\right] \operatorname{erfc}\left(\frac{\sqrt{\tau/\lambda_{\text{e}}}\,\psi}{2a\sqrt{1-\psi^2}}\right) \frac{\mathrm{d}\psi}{\psi^{\nu+1}} \tag{3.132}$$

$$\nu = \frac{Q C_{\text{w}}}{4\pi m \lambda_{\text{m}}} \text{ and } \bar{r} = 2r/m \tag{3.133}$$

Figure 3.29 shows the temperature response for the case considering radial flow. Avdonin (1964) and Malofeev (1960) account for heat transfer within the confining layers. Hence, there is higher dissipation of heat.

There are other approaches that consider a finite length of the overlying layer (Chen and Reddell 1983; Voigt and Haefner 1987) and surface heat exchange (Güven et al. 1983).

The **coded functions** (MATLAB script) of Equations 3.128, 3.131, and 3.132 are listed as *T_guimera.m*, *T_lau_radial.m*, and *T_avd_radial.m*, respectively. As an example, Figure 3.30 shows the temperature response at a radial distance of 1 m away from the injection well.

3.2.4 Natural background groundwater flow

To our knowledge, there is no exact analytical solution to simulate the temperature response of an aquifer considering an injection well and natural background groundwater flow. Therefore, we can only use in an approximation the closest exact analytical solutions for closed systems.

By considering the following energy relationship:

$$q_{tb} = \frac{QC_{\mathrm{w}} \cdot (T_{\mathrm{inj}} - T_0)}{m} \tag{3.134}$$

Equation 3.50, for instance, can be used, resulting in the following equation:

$$T(x,y,t) = T_0 + \frac{QC_{\mathrm{w}}(T_{\mathrm{inj}} - T_0)}{4\pi m C_{\mathrm{m}}\sqrt{D_{\mathrm{t,L}} D_{\mathrm{t,T}}}} \exp\left[\frac{u_{\mathrm{t}} x}{2D_{\mathrm{t,L}}}\right] \times \int_{\left(\frac{x^2}{4D_{\mathrm{t,L}}}+\frac{y^2}{4D_{\mathrm{t,T}}}\right)}^{\infty} \exp\left[-\psi - \left(\frac{x^2}{D_{\mathrm{t,L}}}+\frac{y^2}{D_{\mathrm{t,T}}}\right)\frac{u_t^2}{16 D_{\mathrm{t,L}}\psi}\right]\frac{\mathrm{d}\psi}{\psi} \tag{3.135}$$

Making use of the **Hantush approximation**:

$$W(a_1,a_2) = \sqrt{\frac{\pi}{2a_2}}\exp(-a_2)\,\mathrm{erfc}\left[-\frac{a_2 - 2a_1}{2\sqrt{a_1}}\right] \tag{3.136}$$

we can express Equation 3.135 as follows:

$$T(x,y,t) = T_0 + \frac{QC_{\mathrm{w}} \cdot (T_{\mathrm{inj}} - T_0)}{4mC_{\mathrm{m}}\sqrt{\pi D_{\mathrm{t,T}} u_{\mathrm{t}} r}} \exp\left[\frac{u_{\mathrm{t}} \cdot (x - r)}{2D_{\mathrm{t,L}}}\right]\mathrm{erfc}\left[\frac{r - u_{\mathrm{t}} t}{2\sqrt{D_{\mathrm{t,L}} t}}\right] \tag{3.137}$$

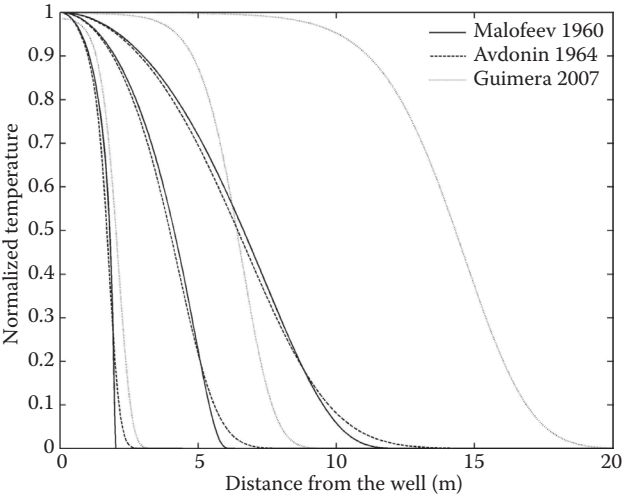

Figure 3.29 Normalized temperature $\bar{T} = (T - T_0)/(T_{inj} - T_0)$ as a function of distance for radial flow equations (Q = 9 m³ day⁻¹, m = 1 m, $\lambda_m = \lambda_{m2}$ = 2.5 W m⁻¹ K⁻¹). Temperature profiles shown at 1, 10, and 50 days.

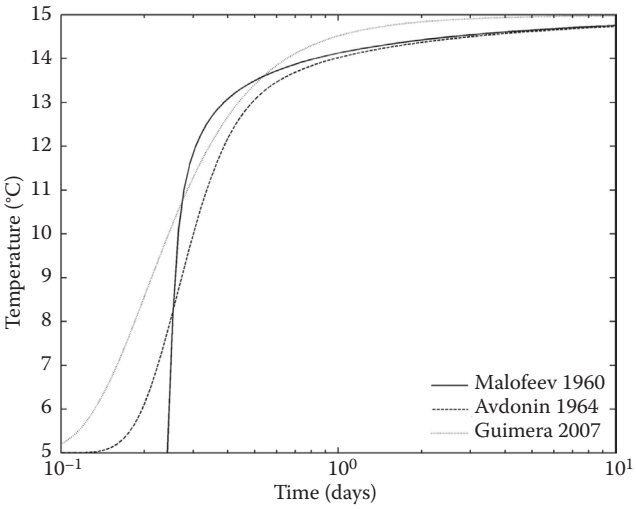

Figure 3.30 Temperature response over time at a radial distance of 1 m from injection well (Q = 9 m³ day⁻¹, m = 1 m, $\lambda_m = \lambda_{m2}$ = 2.5 W m⁻¹ K⁻¹). Equation 3.128: Guimerà et al. (2007); Equations 3.122 and 3.131: Malofeev (1960); Equation 3.132: Avdonin (1964).

where $r = \sqrt{x^2 + y^2 D_{t,L}/D_{t,T}}$. Assuming $\lambda_m = 0$, the above equation is reduced to the equation given by (Keim and Lang 2008)

$$T(x,y,t) = T_0 + \frac{Q C_w \cdot (T_{inj} - T_0)}{4mC_m\sqrt{\pi\beta_T u_t}} \exp\left[\frac{x-r}{2\beta_L}\right] \frac{1}{\sqrt{r}} \operatorname{erfc}\left[\frac{r - u_t t}{2\sqrt{u_t \beta_L t}}\right] \qquad (3.138)$$

This analytical solution is currently used as a regulatory tool for installation, design, and management of open-loop systems in the Federal State of Baden-Württemberg, Germany (Baden-Württemberg 2009).

Using this approach, thermal plume lengths due to heat advection and conduction can be estimated. As explained before, however, this procedure does not consider the hydraulic influence of the injection well.

There are other approximations that account for groundwater flow. Kobus and Mehlhorn (1980), for instance, develop a two-dimensional analytical approximation for simulating transient axial heat conduction through the confining layers of a confined aquifer due to groundwater heat pump systems. The groundwater flow velocity is used for calculating the distance from the source location to a hypothetical line that represents the border between the natural groundwater streamlines and the streamlines diverted due to the local gradient around the injection well. Rauch (1992) developed an analytical formulation for heat transport in aquifers using the groundwater velocity parameter similar to Kobus and Mehlhorn. Additionally, based on a deviation angle of the groundwater flow direction and thermal dispersive transport analyses, the lateral temperature distribution in porous media due to heat conduction is predicted. The basic approach of the previous method is presented by Ingerle (1988) and is currently used in a regulatory guideline of the Austrian Association for Water and Waste Management (ÖWAV 2009).

REFERENCES

Abramowitz, M., Stegun, I.S. (1964). *Handbook of Mathematical Functions. With Formulas, Graphs and Mathematical Tables*. Dover Publ., (1980) Inc., New York, 1046p.

Avdonin, N.A. (1964). Some formulas for calculating the temperature field of a stratum subject to thermal injection. *Izvestijavyssichucebnychzavedenij/Neft' igaz* 7(3), 37–41.

Baden-Württemberg (2009). *Leitfaden zur Nutzung von Erdwärme mit Grundwasserwärmepumpen*. Federal State of Baden-Württemberg, Germany.

Bandos, T.V., Montero, Á., Fernádez, E., Santander, J.L.G., Isodro, J.M., Pérez, J., de Córdoba, P.J.F., Urchueguía, J.F. (2009). Finite line-source model for borehole heat exchangers: Effect of vertical temperature variations. *Geothermics* 38, 263–270.

Beck, M., Bayer, P., de Paly, M., Hecht-Mendez, J., Zell, A. (2013). Geometric arrangement and operation mode adjustment in low enthalpy geothermal fields for heating. *Energy* 49,434–443.

Bear, J. (1979). *Hydraulics of Groundwater*. McGraw-Hill, New York.

Bernier, M.A., Pinel, P., Labit, R., Paillot, R. (2004). A multiple load aggregation algorithm for annual hourly simulations of GCHP systems. *HVAC&R Research* 10, 471–487.

BLOCON (2008). Earth Energy Designer 3.0. BLOCON, Lund, Sweden. Current Version 3.16.

Bredehoeft, J.D., Papadopulos, I.S. (1965). Rates of vertical groundwater movement estimated from the earth's thermal profile. *Water Resources Research* 1, 325–328.

Bundschuh, J. (1993). Modeling annual variations of spring and groundwater temperatures associated with shallow aquifer systems. *Journal of Hydrology* 142, 427–444.

Burger, A., Recordon, E., Bovet, D., Cotton, L., Saugy, B. (1984). *Thermique des nappes souterraines*. Presses Polytechniques Romandes, EPFL, Lausanne, Switzerland.

Carslaw, H.S., Jaeger, J.C. (1946). *Conduction of Heat in Solids*. 1st ed., Oxford University Press, Oxford, UK.

Carslaw, H.S., Jaeger, J.C. (1959). *Conduction of Heat in Solids*. 2nd ed., Oxford University Press, Oxford, UK.

Chaudhry, M.A., Zubair, S.M. (1994). Generalized incomplete gamma functions with applications. *Journal of Computational and Applied Mathematics* 55(1), 99–123.

Chen, C.-S., Reddell, D.L. (1983). Temperature distribution around a well during thermal injection and a graphical technique for evaluating aquifer thermal properties. *Water Resources Research* 19(2), 351–363.

Cui, P., Yang, H., Fang, Z. (2006). Heat transfer analysis of ground heat exchangers with inclined boreholes. *Applied Thermal Engineering* 26, 1169–1175.

DaCosta, J.A., Bennett, R.R. (1960). The pattern of flow in the vicinity of a recharging and discharging pair of wells in an aquifer having areal parallel flow. IAHS Publ. No. 52, pp. 524–536.

Diao, N., Li, Q., Fang, Z. (2004). Heat transfer in ground heat exchangers with groundwater advection. *International Journal of Thermal Sciences* 43(12), 1203–1211.

Domenico, P.A., Palciauskas, V.V. (1973). Theoretical analysis of forced convective heat transfer in regional ground-water flow. *Geological Society of America Bulletin* 84, 3803–3814.

Eskilson, P. (1987). Thermal analysis of heat extraction boreholes. Ph.D. Thesis Univ. of Lund, Lund, Sweden.

Eskilson, P., Claesson, J. (1988). Simulation model for thermally interacting heat extraction boreholes. *Numerical Heat Transfer* 13, 149–165.

Gelhar, L.W., Collins, M.A. (1971). General analysis of longitudinal dispersion in nonuniform flow. *Water Resources Research* 7(6), 1511–1521.

GLHEPRO (2007). GLHEPRO 4.0 for Windows User's guide. School of Mechanical and Aerospace Engineering Oklahoma State University. Distributed by the International Ground Source Heat Pump Association.

Gringarten, A.C., Sauty, J.P. (1975). A theoretical study of heat extraction from aquifers with uniform regional flow. *Journal of Geophysical Research* 80(35), 4956–4962.

Gröber, H., Erk, S., Grigull, U. (1955). *Grundgesetze der Wärmeübertragung*. U. Grigull (rev. ed.), Springer, Berlin, Germany.

Guimerà, J., Ortuño, F., Ruiz, E., Pérez-Paricio, A. (2007). Influence of ground-source heat pumps on groundwater. *Conference Proceedings*, European Geothermal Congress, Unterhaching, Germany, 30 May–1 June 2007.

Güven, O., Melville, J.G., Molz, F.J. (1983). An analysis of the effect of surface heat exchange on the thermal behavior of an idealized aquifer thermal energy storage system. *Water Resources Research* 19(3), 860–864.

Häfner, F., Sames, D., Voigt, H.D. (1992). *Wärme- und Stofftransport*. Springer Verlag, Berlin.

Ham, P.A.S., Schotting, R.J., Prommer, H., Davis, G.B. (2004). Effects of hydrodynamic dispersion on plume lengths for instantaneous bimolecular reactions. *Advances in Water Resources*, 27(8), 803–813.

Hecht-Méndez, J., de Paly, M., Beck, M., and Bayer, P. (2013). Optimization of energy extraction for vertical closed-loop geothermal systems considering groundwater flow. *Energy Conversion and Management*, 66, 1–10.

Hellström, G. (1991). Ground heat storage. Thermal analyses of duct storage systems. PhD Thesis, Lund University, Lund, Sweden.

Huber, A. (2008). *Software Manual Program EWS Version 4.0 Calculation of Borehole Heat Exchangers*. Huber Energietechnik AG, Zurich, Switzerland.

Incropera, F.P., Dewitt, D.P., Bergman, T.L., Lavine, A.S. (2007). *Introduction to Heat Transfer*. 5th ed., J. Wiley & Sons, Hoboken, N.J., USA.

Ingerle, K. (1988). Beitrag zur Berechnung der Abkühlung des Grundwasserkörpers durch Wärmepumpen. *Österreichische Wasserwirtschaft* 40, 11(12).

Ingersoll, L.R., Zobel, O.J., Ingersoll, A.C. (1948). *Heat Conduction; with Engineering, Geological and Other Applications*. 1st ed., McGraw-Hill, New York, 278p.

Ingersoll, L.R., Zobel, O.J., Ingersoll, A.C. (1954). *Heat Conduction; with Engineering, Geological and Other Applications*. Rev. and ext. ed., McGraw-Hill, New York, 325p.

Keim, B., Lang, U. (2008). *Thermische Nutzung von Grundwasser durch Wärmepumpen*. Umweltministerium Baden-Württemberg, State of Baden-Württemberg, Stuttgart, Germany.

Kobus, H., Mehlhorn, H. (1980). Beeinflussung von Grundwassertemperaturen durch Wärmepumpen. *gwf Wasser Abwasser* 121(6), 261–268.

Lamarche, L., Beauchamp, B. (2007). A new contribution to the finite line-source model for geothermal boreholes. *Energy and Buildings* 39(2), 188–198.

Lauwerier, H.A. (1955). The transport of heat in an oil layer caused by the injection of hot fluid. *Applied Scientific Research, Section A,* 5 (2–3) 145–150. Lippmann, M.J., Tsang, C.F. (1980). Ground-water use for cooling: Associated aquifer temperature changes. *Ground Water* 18(5), 452–458.

Lu, N., Ge, S. (1996). Effect of horizontal heat and fluid flow on the vertical temperature distribution in a semiconfining layer. *Water Resources Research* 32(5), 1449–1453.

Malofeev, G.E. (1960). Calculation of the temperature distribution in a formation when pumping hot fluid into a well. *Neft'I Gaz* 3(7), 59–64.

Man, Y., Yang, H., Diao, N., Liu, J., Fang, Z. (2010). A new model and analytical solutions for borehole and pile ground heat exchangers. *International Journal of Heat and Mass Transfer* 53(13–14), 2593–2601.

Marcotte, D., Pasquier, P., Sheriff, F., Bernier, M. (2010). The importance of axial effects for borehole design of geothermal heat-pump systems. *Renewable Energy* 35(4), 763–770.

Mehlhorn, H., Spitz, K.-H., Kobus, H. (1981). Kurzschlussströmung zwischen Schluck- und Entnahmebrunnen – Kritischer Abstand und Rückströmrate. *Wasser und Boden* 33(4) 170–174.

Mercer, J.W., Faust, C.R., Miller, W.J., Pearson Jr., F.J. (1982). Review of simulation techniques for aquifers thermal energy storage (ATES). In VenTe Chow (Editor), Advances in Hydroscience, 13, 1–129. Academic Press, New York, USA.

Metzger, T., Didierjean, S., Maillet, D. (2004). Optimal experimental estimation of thermal dispersion coefficients in porous media. *International Journal of Heat and Mass Transfer* 47(14–16), 3341–2253.

Michopoulos, A., Kyriakis, N. (2009). Predicting the fluid temperature at the exit of the vertical ground heat exchangers. *Applied Energy* 86, 2065–2070.

Mikhailov, M.D., Özisik, M.N. (1984). *Unified Analysis and Solutions of Heat and Mass Diffusion*. J. Wiley & Sons, New York, USA.

Molina-Giraldo, N., Bayer, P., Blum, P. (2011a). Evaluating the influence of thermal dispersion on temperature plumes from geothermal systems using analytical solutions. *International Journal of Thermal Sciences* 50(7), 1223–1231.

Molina-Giraldo, N., Zhu, K., Blum, P., Bayer, P., Fang, Z. (2011b). A moving finite line source model to simulate borehole heat exchangers with groundwater advection. *International Journal of Thermal Sciences* 50(12), 2506–2513.

Nagano, K., Katsura, T., Takeda, S. (2006). Development of a design and performance prediction tool for ground source heat pump system. *Applied Thermal Engineering* 26, 1578–1592.

ÖWAV (2009). Thermische Nutzung des Grundwassers und des Untergrunds—Heizen und Kühlen (Thermal use of groundwater and underground—Heating and cooling). ÖWAV-Regelblatt 207, Österreichischer Wasser- und Abfallwirtschaftsverbands ÖWAV (Guideline 207 of the Austrian Water and Waste Management Association), Vienna, Austria.

Philippe, M., Bernier, M., Marchio, D. (2009). Validity ranges of three analytical solutions to heat transfer in the vicinity of single boreholes. *Geothermics* 38(4), 407–413.

Rauch, W. (1992). Ausbreitung von Temperaturanomalien im Grundwasser. Veröffentlichung Univ. Innsbruck No. 188.

Signorelli, S., Bassetti, S., Pahud, D., Kohl, T. (2007). Numerical evaluation of thermal response tests. *Geothermics* 36(2), 141–166.

Spillette, A.G. (1965). Heat transfer during hot injection into an oil reservoir. *Journal of Canadian Petroleum Technology* 4(4), 213–218.

Sutton, M.G., Nutter, D.W., Couvillion, R.J. (2003). A ground resistance for vertical bore heat exchangers with groundwater flow. *Journal of Energy Resources Technology ASME* 125(3), 183–189.

Tóth, J. (1963). A theoretical analysis of groundwater flow in small drainage basins. *Journal Geophysical Research* 68(16) 4795–4812.

Trüeb, E. (1976). Die Bedeutung des Grundwassers für die Versorgung der Schweiz. DVGW-Schriftenreihe Wasser 10.

Uffink, G.J.M. (1983). Dampening fluctuations in groundwater temperature by heat exchange between the aquifer and the adjacent layers. *Journal of Hydrology* 60, 311–328.

Voigt, H.D., Haefner, F. (1987). Heat transfer in aquifers with finite caprock thickness during a thermal injection process. *Water Resources Research* 23(12), 2286–2292.

Woods, K., Ortega, A. (2011). The thermal response of an infinite line of open-loop wells for ground coupled heat pump systems. *International Journal of Heat and Mass Transfer* 54, 5574–5587.

Yang, S.Y., Yeh, H.D. (2008). An analytical solution for modeling thermal energy transfer in a confined aquifer system. *Hydrogeology Journal* 16, 1507–1515.

Zeng, H.Y., Diao, N.R., Fang, Z.H. (2002). A finite line-source model for boreholes in geothermal heat exchangers. *Heat Transfer Asian Research* 31(7), 558–567.

Zubair, S., Chaudhry, M. (1996). Temperature solutions due to time-dependent moving-line heat sources. *Heat Mass Transfer* 32(3), 185–189.